ARE THE MANTLE LITHOSPHERE AND LOWER CRUST PREFERENTIALLY THINNED DURING CONTINENTAL RIFTING?

by

KALYN J. TEW

ANDREW MARK GOODLIFFE, COMMITTEE CHAIR
SAMANTHA HANSEN
DELORES ROBINSON
JACK PASHIN

A THESIS

Submitted in partial fulfillment of the requirements
for the degree of Master of Science in the
Department of Geological Sciences
in the Graduate School of
The University of Alabama

TUSCALOOSA, ALABAMA

2018

ABSTRACT

Worldwide, estimates of extension in rift zones vary greatly depending on the method used to calculate the extension. This variability is the result of the discrepancy between different methodologies and may be the result of polyphase faulting, subresolution faulting, and/or depth-dependent extension. Such inconsistency between estimates has been noted in the Woodlark Basin, an active transition zone between continental rifting and seafloor spreading. Previous work in the basin, where seafloor spreading has not initiated, calculated extension by summing fault heaves, calculating subsidence, and determining plate motion from Euler pole kinematics, yielding estimates of 111 km (±23) from brittle extension, 115 km (±47) from subsidence, and 200 km (±40) from Euler pole kinematics (Kington and Goodliffe, 2008). By incorporating polyphase and subresolution faulting into the brittle extension estimate, Kington and Goodliffe (2008) resolved the discrepancy between estimates of extension derived from brittle faulting and subsidence. The third method used to estimate extension, Euler pole kinematics, produced a large discrepancy. Kington and Goodliffe (2008) interpreted this to be the result of preferential extension of the lower crust and mantle lithosphere during the rifting phase and proposed that uniform extension would occur throughout the lithosphere after seafloor spreading initiation. The current study explores potential errors in previous work in the basin and determines if the results are applicable to other portions of the basin. In contrast to Kington and Goodliffe (2008), the current study determines extension where seafloor spreading initiated at ~0.8 Ma. Using the methods and associated errors from Kington and Goodliffe (2008), Euler pole extension estimates (~202 to 238 km) are ~2 times higher than brittle (~69 to 90 km) and subsidence (~60 to 79 km) extension estimates, consistent with the previously seen discrepancy. When taking into

account other sources of error not considered by Kington and Goodliffe (2008), the current study shows the previous methods lack the constraints necessary to produce conclusive results. This would also render the results of the previous study by Kington and Goodliffe (2008) inconclusive. Therefore, it is not necessary to invoke the Kington and Goodliffe (2008) model to explain rifting in the western Woodlark Basin.

Key words: lithospheric extension, sea-floor spreading, continental rifting, rifting to spreading transition zone, extension estimates, Woodlark Basin, Papua New Guinea

LIST OF ABBREVIATIONS AND SYMBOLS

~	Approximately
ρ	Density
β	Stretching factor
α	Thermal coefficient
Ma	Mega-annum (Million years before present)
Myr	Million years
mW	Milliwatt
m	Meter
km	Kilometer
E	East
W	West
N	North
S	South
$mm.yr^{-1}$	Millimeters per year
$kg.m^{-3}$	Kilograms per meter cube
C	Celsius
sec	Seconds
ms	Milliseconds
h_{sb}	Thickness of sedimentary basin

h_{cc}	Pre-rift lithospheric thickness
ρ_m	Mantle density
ρ_{cc}	Crustal Density
ρ_s	Density of basin infill
α_v	Thermal coefficient of mantle
T_0	Surface temperature
T_1	Upper asthenosphere temperature
β	Crustal thinning factor
lcc	Pre-rift thermal lithospheric thickness
S_i	Initial subsidence
ρ_c	Density of crust
π	Pi
λ	Wavelength
v	Velocity
f	Frequency

ACKNOWLEDGEMENTS

First, I would like to thank my thesis advisor, Dr. Andrew Goodliffe, and my entire thesis committee, Dr. Samantha Hansen, Dr. Jack Pashin, and Dr. Delores Robinson, for their valuable input into this study. I would also like to thank the faculty, staff, and students in the Department of Geological Sciences for all of their support, especially Berg Nazlim for his help with Matlab®.

I would like to thank my parents, Nick and Rhonda Tew, and my grandparents, Berry and Edna Tew, for their love and support throughout my educational career. Without them, I would not be where I am today.

The University Scholars program allowed me to begin graduate school with financial support from my Presidential Scholarship, which I am thankful for. I would like to thank the Department of Geological Sciences for their financial support through my teaching assistantship. I am thankful to the family of Dr. Jen Ho Fang, who provided a research scholarship, the Johnson Fund, and the Graduate School for supporting my trip to the 2017 Geological Society of America Annual Meeting in Seattle, WA, to present my research.

CONTENTS

LIST OF TABLES

LIST OF FIGURES

CHAPTER 1: INTRODUCTION

Rift zones show a discrepancy between extension estimates determined through different methods. For instance, Davis and Kuznir (2004) proposed that in the Goban Spur, the Galacia Bank, the Vøring Sea, and the South China Sea rift basins the discrepancy between upper crustal stretching and whole lithospheric stretching at rifted margins results from depth-dependent stretching. To test this hypothesis, their study used three different methods to estimate extension during rifting: 1) summing fault heaves from seismically imaged faults; 2) deriving whole crustal stretching from seismic reflection, refraction, and gravity inversion; and 3) determining whole lithospheric stretching from subsidence estimations. To sum fault heaves, Davis and Kuznir (2004) used basement imaged faults from 2-D seismic reflection surveys and noted that the upper crustal extension derived from this method would be underestimated if polyphase faulting, subseismic faulting, fault geometry, and rifting that began above sea level were ignored. Whole crustal stretching and thinning were calculated by using wide-angle seismic studies and gravity surveys to determine present day crustal thickness in the rift basins. Comparing this thickness to the initial crustal thickness allowed Davis and Kuznir (2004) to determine a thinning factor for the crust. Whole lithospheric stretching and thinning were determined based on evidence of subsidence history recorded in the stratigraphy of the basins. This evidence was used to develop a 2-D backstripping, decompaction, and post-breakup thermal model for subsidence that assumed uniform stretching. Davis and Kuznir (2004) determined that in the Goban Spur, the Galacia Bank, and the South China Sea, the whole crustal stretching factor is greater than the upper crustal stretching factor. In the Goban Spur, extension estimated from the upper crustal extension estimate was 12 km (±5); the estimate from the whole crustal thinning extension

estimate was 42 km (±8). In the Galacia Bank, the upper crustal extension estimate was 80 km (±8); the whole crustal thinning extension estimate was 203 km (±27). In the South China Sea, the upper crustal extension estimate was 55 km (±10), while the whole crustal extension estimate was 140 km (±25). In the Vøring Sea, the whole lithospheric stretching factor (1.0 to 2.0) is greater than the upper crustal stretching factor (1.07 ±0.03). In all cases, Davis and Kuznir (2004) concluded that these results were evidence of depth-dependent stretching adjacent to the continental-ocean boundary.

Expanding on the work of Davis and Kuznir (2004), Kington and Goodliffe (2008) examined potential sources of error in the associated methods using data from the Woodlark Basin, focusing on a portion of the basin where seafloor spreading has not yet initiated. Incorporating polyphase and subseismic resolution faulting into the extension determined from seismically imaged faults provided a larger brittle (upper crustal) extension estimate that agreed with that derived from subsidence (whole crustal). Specifically, these estimates of extension were 111 km (±23) from brittle extension and 115 km (±47) from subsidence. A third method, Euler pole kinematics, was also used (Taylor et al., 1999). This method is a measure of entire plate (whole lithosphere) motion. Euler pole solutions were derived from magnetic chron 2A.3n (3.33 Ma to 3.58 Ma; Cande and Kent, 1995) to the present. Kington and Goodliffe (2008) used the Euler pole results from Taylor et al. (1999) and found even greater extension across the Woodlark Basin (200 km ± 40). To explain the discrepancy between methods, Kington and Goodliffe (2008) proposed a model with higher rates of extension in the lower crust and mantle lithosphere. In that model, the upper crust is decoupled from the lower crust, allowing the upper crust to extend at slower rates until the initiation of seafloor spreading breaches the lithosphere.

Once seafloor spreading has initiated, extension proceeds at a uniform rate throughout the lithosphere (Figure 1).

The current study follows the methods of Kington and Goodliffe (2008) in a part of the Woodlark Basin (between 152°E and 153°E) where seafloor spreading has initiated. This allows

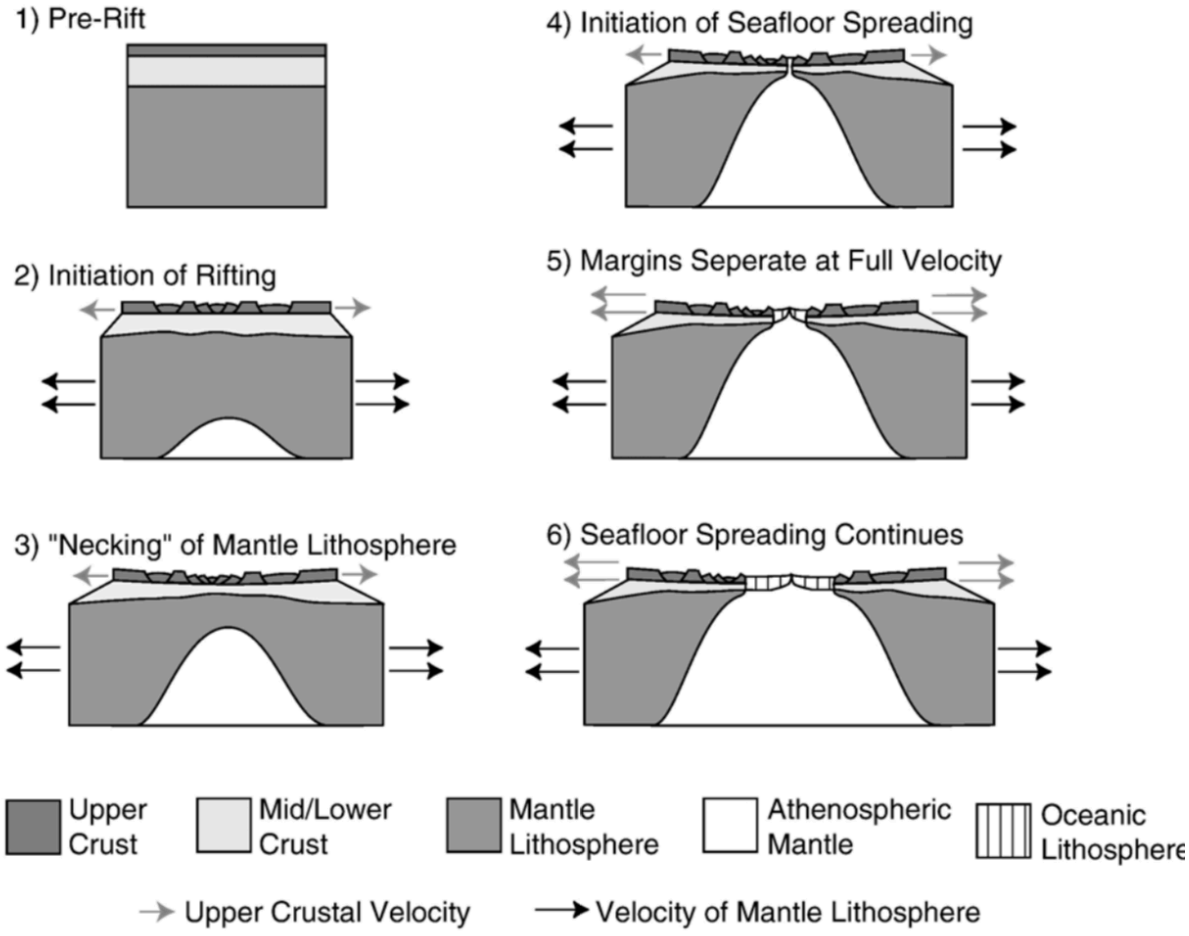

Figure 1. Lithospheric extension model from Kington and Goodliffe (2008). In this model, the brittle upper crust and ductile mantle lithosphere are detached during continental extension. It is only after the initiation of seafloor extension that the upper crust and mantle lithosphere are moving at the same rate.

for examination of an area that has completed the rifting phase of extension; therefore, total extension due to continental rifting along a north-south profile can be attained. Kington and Goodliffe (2008) did not take various, potentially impactful sources of error into account during

their study. These potential errors include underestimating sediment cover, ignoring metamorphic core complexes, assuming no flexural rigidity, assuming conservation of area during rifting, assuming that the basin began rifting at sea level, and assuming Euler pole spreading rates are accurate back to 6 Ma. This study examines these sources of error by determining the impact of these variables on extension rates. The current study indicates that Kington and Goodliffe (2008) were correct in their hypothesis that incorporating polyphase and subresolution faulting into brittle extension estimates greatly increases the amount of extension observed in a rift zone. However, when the sources of error are incorporated, the Kington and Goodliffe (2008) model may not be necessary to explain the results, as there are several uncertainties associated with the different extension estimates.

CHAPTER 2: GEOLOGICAL BACKGROUND

2.1: Geologic Setting in the Woodlark Basin

The ~900 km long Woodlark Basin is located in the southwestern Pacific Ocean at the juncture of the Woodlark and Australian plates (Figure 2). The Woodlark Plate is moving north relative to the Australian Plate at >20 mm yr^{-1} (Little et al., 2007), with extension accommodated by continental rifting and the accretion of oceanic lithosphere. The Woodlark Basin is bordered to the south by the Pocklington Trough, the trench formed when the Australian plate subducted beneath Papua New Guinea in Late Cretaceous time (Figure 2; Taylor and Huchon, 2002). Partial subduction of the Papuan Plateau, a rifted fragment of the Australian continent, resulted in obduction of an ophiolite suite, the Papuan Ultramafic Belt, in the Late Paleocene to Early Oligocene (Davies and Jaques, 1984). The Papuan Ultramafic Belt forms the backbone of the Papuan Peninsula and underlies much of the Woodlark Basin. The Trobriand Trough (Figure 2), a trench formed by subduction of the Solomon Plate beneath the Woodlark Basin region, borders the Woodlark Basin to the north. Subduction created a magmatic arc active from Miocene time to the present (Davies and Smith, 1971). Bordering the basin to the west, the metamorphic core complexes of the D'Entrecasteaux Islands have been forming since Late Miocene time (Martinez et al., 2001). The Nubara Fault is a large active transform fault bordering the Woodlark Plate to the northeast and separating it from the Solomon Sea. To the north, the Nubara Fault terminates at the San Cristobal Trench, which bounds the Woodlark Basin to the east (Figure 2). In their discussion, Kington and Goodliffe (2008) suggested that if the Nubara Fault extends east into the Woodlark Rise, on the northern side of the Woodlark Basin, a third plate would be predicted, the

Trobriand Plate. This interpretation is supported by earthquake fault plane solutions (Abers et al., 1997). At the location of their study (Figure 2, white box), the presence of a third plate would

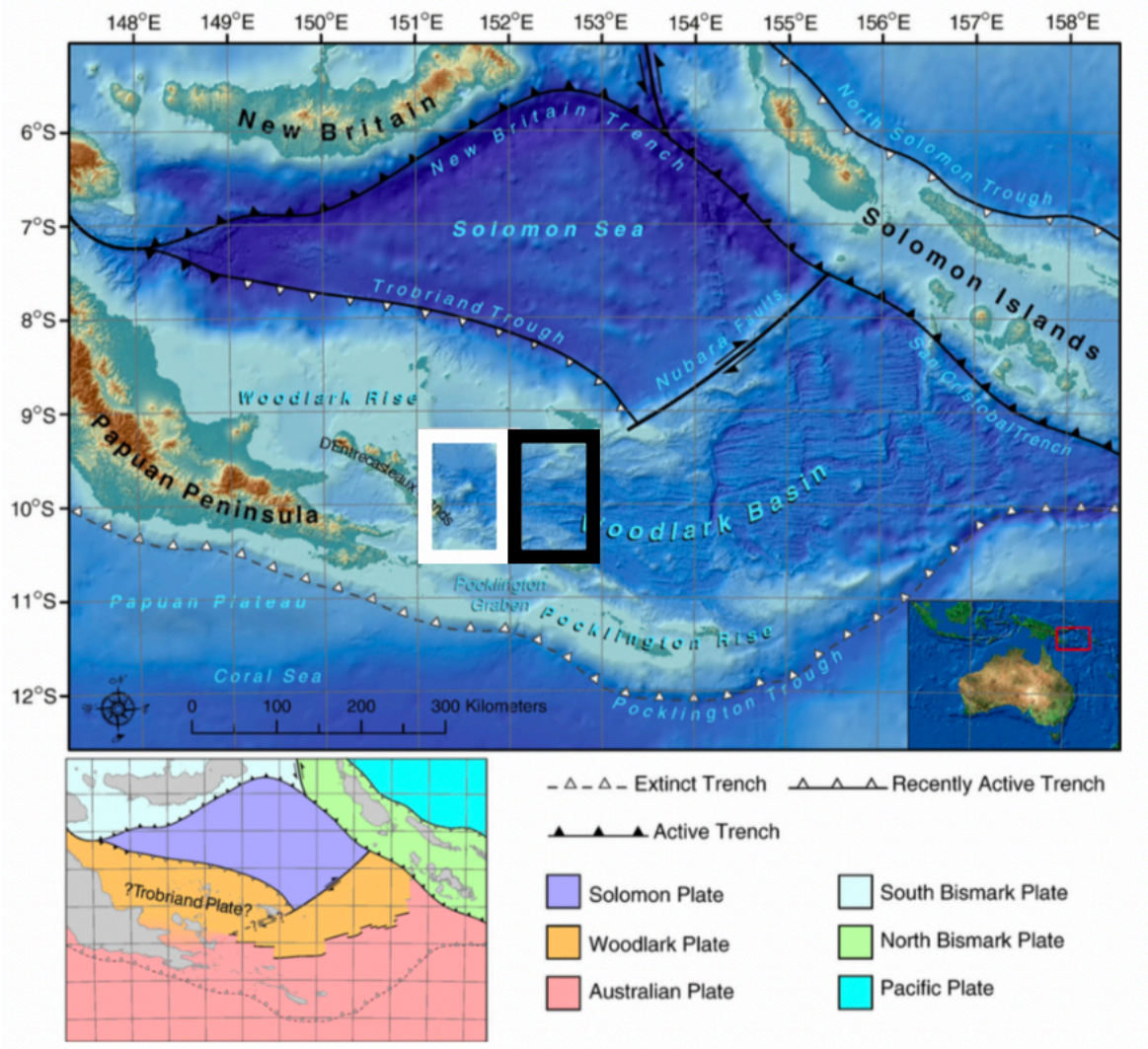

Figure 2. Map of the Woodlark Basin region, modified from Kington and Goodliffe (2008). The basin is bounded by the Pocklington Trough to the south, the Papuan Peninsula to the west, the Trobriand Trough and Nubara Fault to the north, and the San Cristobal Trench to the east. The current study area is outlined in black, with the previous Kington and Goodliffe (2008) study area outlined in white. The location of the Woodlark Basin is shown by the inset in the bottom right corner of the map. The lower left figure shows the known and hypothesized plates.

vastly complicate the Kington and Goodliffe (2008) calculations as the plate would encompass the majority of the northern portion of the study area. Baldwin et al. (1993) proposed that neither

the Nubara Fault nor the Trobriand Trough are active plate boundaries. The focus of the current study is to the east, where less of the northern portion of the study area would be impacted by the potential Trobriand Plate.

Rifting began in the Woodlark Basin at 8.4 Ma (Taylor and Huchon, 2002). Seafloor spreading initiated in the easternmost spreading segment between ~5.89 and ~6.14 Ma (Taylor et al., 1999), and it is currently propagating westward at 140 km Myr^{-1} (Taylor and Huchon, 2002). Taylor et. al (1999) determined the rate of total plate motion in the Woodlark Basin using Euler pole kinematics. Using transform fault azimuths, magnetic chron data, and other geological markers, Taylor et al. (1999) proposed two Euler poles to describe the opening of the basin (Figure 3). Rotation about the first Euler pole (9.3˚(±0.2°) S, 147° (+1°-2°) E with an angular

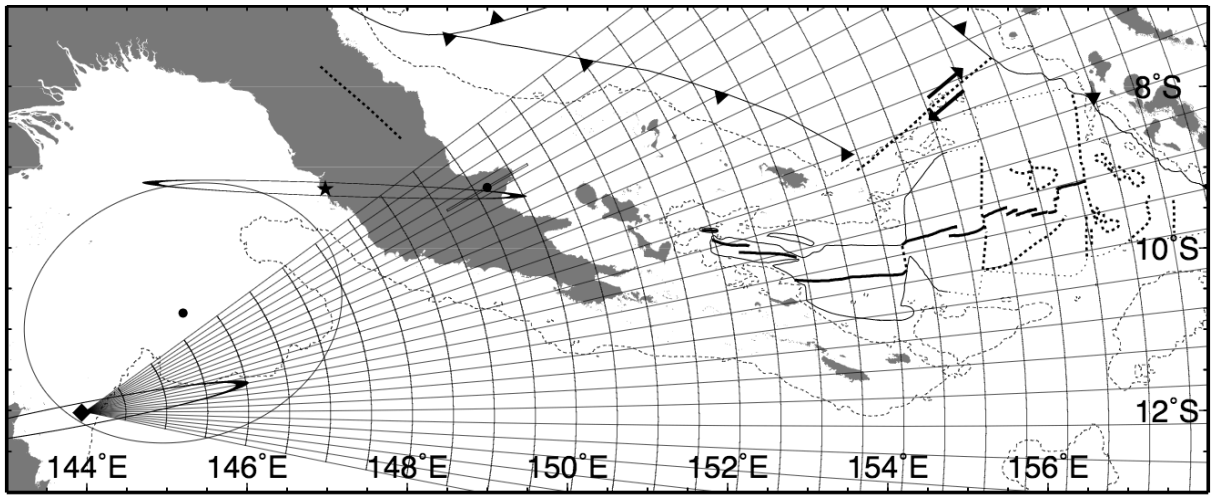

Figure 3. Euler pole locations in the basin. The black diamond represents the current Euler pole, and the black star represents the pre-0.5 Ma Euler pole. Ellipses represent the 95% confidence intervals. Strike-slip fault movement is shown with black arrows. Subduction is indicated by a black line with triangles on the down-going plate. Land above sea level is shown in dark grey. Thick black line segments indicate the location of the spreading center. Thin black lines show the continent-ocean boundary. Gray dotted lines indicate when bathymetry reaches a 2000 km depth. Black dotted lines represent transform fault traces.

velocity of 4.234˚Myr^{-1}) was active until 0.5 Ma. A switch to the modern Euler pole (12°S,

144°E with an angular velocity of 2.437° Myr^{-1}) at ~0.5 Ma resulted in a major spreading center reorientation at ~80 ka (Goodliffe et al., 1997). Average Brunhes chron seafloor spreading rates vary from 36 to 67 mm yr^{-1} from west to east (Taylor et al., 1999). The basin shows two discrete styles for the rifting-to-spreading transition: nucleation and propagation (Goodliffe et al., 1997). Nucleation of discrete spreading centers is evident between accommodation zones. Following nucleation, spreading segments grow by propagation. This process cuts into the margins and creates characteristic "V" shaped morphologies in map view (Goodliffe, 1998).

For subsidence calculations, crustal thickness must be estimated at the initiation of rifting. The Woodlark and Pocklington rises were split during initial continental rifting, starting at ~8.4 Ma (Taylor and Huchon, 2002). Prior to the initiation of rifting, it is likely that the basin formed along a zone of weakness, continuous with the orogenic belt of the Papuan Peninsula (Taylor and Huchon, 2002). Seismic refraction data (Finlayson et al., 1976) indicated a maximum crustal thickness of ~50 km in the western portion of the basin along the Papuan Peninsula at ~150°E, where there is ~2 km of elevation. Therefore, if the basin was continuous with this orogeny prior to rifting, an initial crustal thickness of 50 km could be assumed. However, there is no direct evidence to support this hypothesis. Based on the core and borehole data from ODP Leg 180, Taylor and Huchon (2002) found stratigraphic evidence of low relief islands, lagoons, swamps, and deltaic sequences after the initiation of rifting at ~8.4 Ma. In addition, Goodliffe et al. (2002) found unconsolidated sediments, dated at ~5.23 Ma to 5.39 Ma, containing brackish water fauna characteristic of a coastal environment, indicating the basin was at sea level during this period of rifting. Therefore, for the current study, as in the case of Kington and Goodliffe (2008), it is assumed that the basin was at sea level at the initiation of rifting. A refraction study in the basin (Abers et al., 1997) showed that continental crust at sea

level is 35 km thick. Receiver functions (Abers et al., 2002) indicate that the continental crust that has undergone the least extension at the margins of the rift basin is 30- 35 km thick. Based on this, for the current study, a pre-rift thickness of 35 km is assumed.

Heat flow in the Woodlark Basin ranges from ~30 to 350 mW m^{-2} (Goodliffe et al., 2000). These variations in heat flow are a result of a variable thermal gradient in the basin that is influenced by the lithospheric thickness. In addition, localized high temperatures result in a lower viscosity lithosphere. An influx of water from the subduction of oceanic crust in the north will lower the melting temperature and further decrease viscosity of the lithosphere. These factors may create conditions for lower crustal flow (McKenzie, 2002). In the absence of significant brittle faulting, including a major crustal detachment, subsidence can most easily be described by the removal of the lower crust through ductile flow (Taylor et al., 1999). Evidence for this process is seen from the subsidence of the largely unfaulted northern margin of the basin at the rifting-to-spreading transition between 151°E and 152°E at ~9°S (Figure 4).

As previously noted, Kington and Goodliffe (2008) estimated the amount of extension during rifting in the Woodlark Basin where seafloor spreading has not yet begun. The current study focuses between 152°E and 153°E, where seafloor spreading initiated at ~0.8 Ma, permitting observation of the extension accommodated during the full continental rifting cycle. The current study area is bounded by the Woodlark Rise to the north and the Pocklington Trough to the south (Figures 2 and 4) and contains sediments less than 1 km thick overlain on easily imaged basement. ODP Leg 180 core data collected west of the current study area shows that sediments are a combination of consolidated and loosely consolidated sedimentary rock, coarse grained clastic sediments, and siliceous ooze (Taylor and Huchon, 2002). Multiple discrete spreading segments are imaged in swath sidescan and bathymetry data (Taylor et al., 1999)

(Figure 4). The westernmost spreading segment (segment 1) has an eastward directed propagation tip located at ~152.8°E, 10.15°S (Taylor et al., 1999). To the south of this spreading center, a westward directed seafloor spreading propagation tip (segment 2) is located at ~152.82°E, 10.39°S (Taylor et al., 1999). The two segments are separated by a continental fault

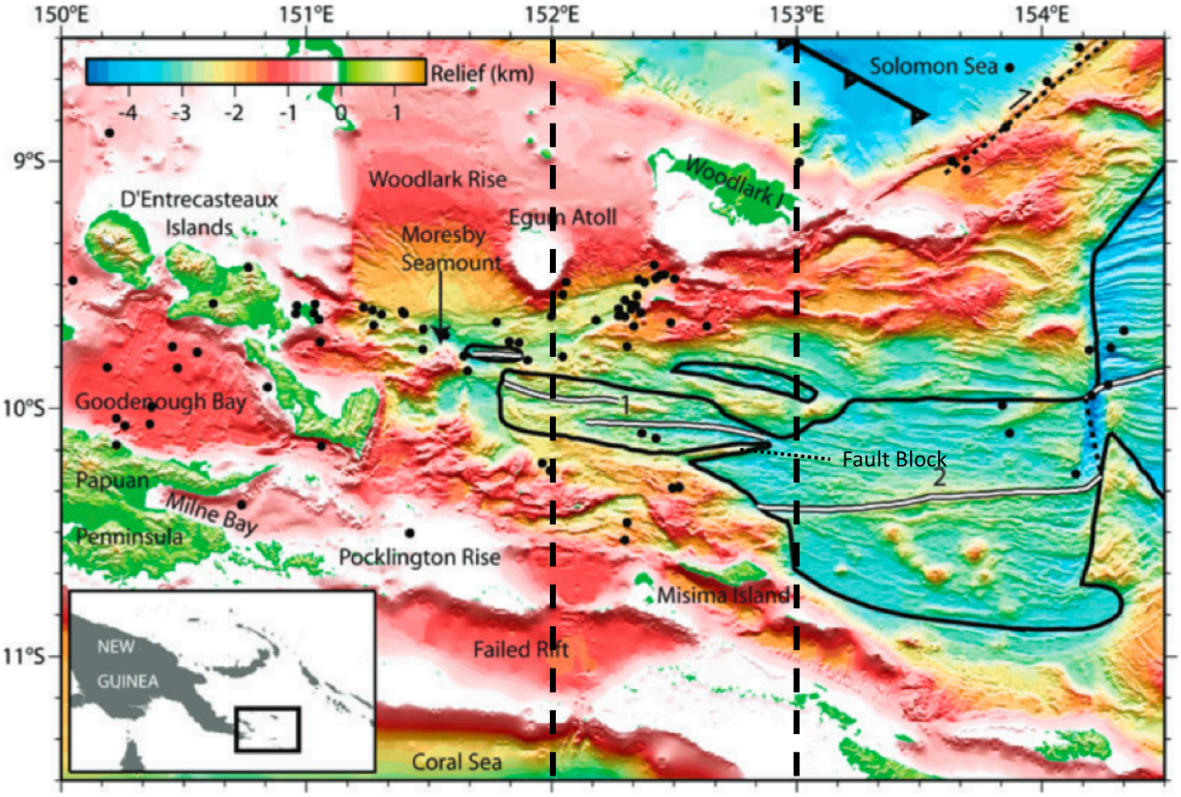

Figure 4. Bathymetry of the Woodlark Basin from Goodliffe and Taylor (2007). The continent-ocean boundary is outlined in black. The color scale (top left) indicates relief in meters. Spreading segments are numbered based on Taylor et al. (1999). The centers of the spreading segments are indicated by the white lines. The study area is located between 152°E and 153°E, as indicated by the black dashed lines. Black dots represent seismicity measured between June 1999 and June 2000. Subduction is indicated by the black line with triangles on the overlying plate. The location of the Woodlark Basin is shown by the inset in the bottom left corner.

block. To the south of these spreading segments, there are predominantly east-west trending basins with ~1 km water depths. Ridges that almost reach sea level are bounded by normal faults dipping 30-50° to the north and south. These basins contain sediment packages that are ~0.5 km

thick (Kington and Goodliffe, 2008). Misima Island is located to the south of spreading segments 1 and 2. To the north of the western end of spreading segment 1 is a 2 km wide basin. Water depths in the basin reach ~2.8 km. To the north, there is a ridge with ~0.7 km water depth containing sediment packages that are 0.5 to 1 km thick. Directly north of this basin and ridge is Egum Atoll. To the north of the eastern end of spreading segment 1, another continental fault block (~11 km wide) bounds more oceanic crust to the north. Further north, two ridges (~60 km long and reaching water depths of 0.4 and 0.2 km, respectively) form the Woodlark Rise. Woodlark Island lies north of this rise.

2.2: Lithospheric Extension

Early rift models do not account for discrepancies in extension between the upper and lower lithosphere. For instance, McKenzie (1978) proposed a pure shear model, which predicted symmetrical rifting of the crust with opening rates that are constant throughout the lithosphere, regardless of depth (Figure 5). The McKenzie (1978) pure shear model includes an approach to

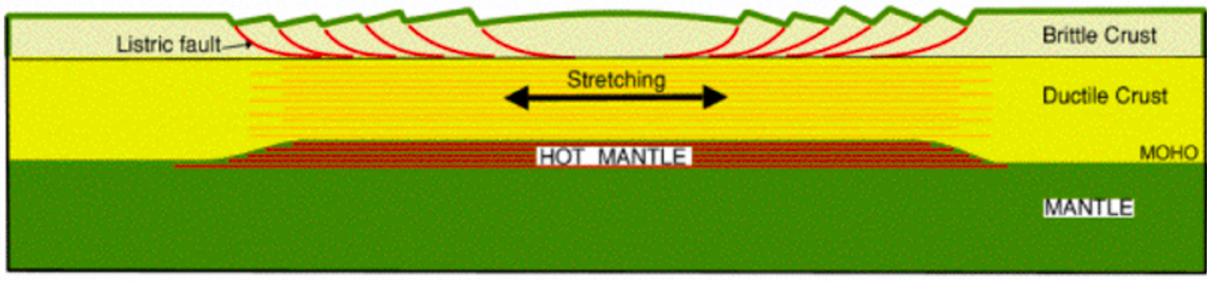

Figure 5. Pure shear rifting model from McKenzie (1978). Heavy black arrows indicate direction of extension. In this model, extension rates are uniform throughout the lithosphere. Symmetric rifts will form along each margin in the upper brittle crust, while thinning and stretching will occur in the ductile lower crust.

estimate extension from subsidence; however, estimates of extension based on this method assume instantaneous rifting, Airy isostasy, and an average geothermal gradient consistent with the continental lithosphere. In contrast, Wernicke (1985) described continental rifting using a

simple shear model, where the focus of extension is asymmetric. Brittle faulting in the upper plate, above a crustal scale detachment, results in less brittle extension evident in the lower plate (Figure 6). Driscoll and Karner (1998) noted that the simple shear model did not explain why in

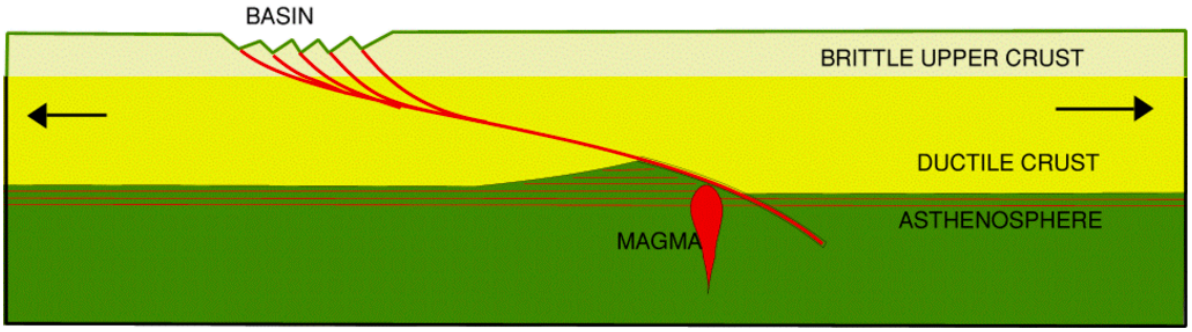

Figure 6. Simple shear rifting model from Wernicke (1985). Arrows indicate direction of extension. Rate of extension is the same at depth throughout the lithosphere, with accommodation for stretching resulting in brittle faulting of the upper plate above a detachment fault extending to the asthenosphere. The lower plate will show little to no brittle extension.

many basins both conjugate margins seem to lack sufficient brittle faulting and are thus interpreted as being part of the lower plate. They termed this problem the "upper-plate paradox." The early models of McKenzie (1978) and Wernicke (1985) focused on end-member solutions. In contrast, Lavier and Manatschal (2006) found evidence of both large-scale symmetric extension (pure shear) and discrete areas of asymmetric extension (simple shear) in the Iberia and Newfoundland margins and developed a new model (Figure 7). Similarly, the Woodlark Basin shows evidence of both pure and simple shear varying in dominance temporally and spatially in the basin (Taylor et al., 1999). A more recent study, Huismans and Beaumont (2014), modeled the lithosphere and determined that depth-dependent extension explains why many rifted margins appear not to follow the end-member rifting models.

Several studies (*e.g.*, Walsh, 1991; Reston, 2005) have suggested explanations for the discrepancies between extension estimates predicted through different methods (Davis and

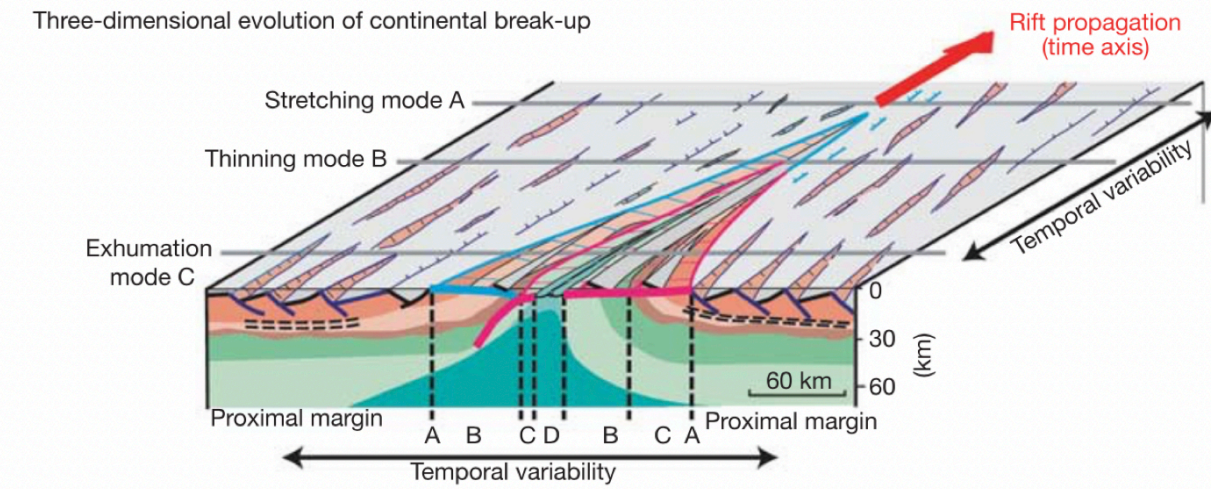

Figure 7. Rifting model from Lavier and Manatschal (2006). Heat flow, rifting geometries, and the amount of thinning vary spatially and temporally. This basin behaves as both pure shear and simple shear.

Kuznir, 2004); these studies were incorporated into Kington and Goodliffe (2008) and resulted in agreement between brittle and subsidence extension estimations. One suggestion was to incorporate subseismic resolution faults into brittle extension estimates. Seismic waves have a frequency (f) related to the wavelength (λ) and velocity (v) of the wave by:

$$v = \lambda f \qquad (1)$$

Given this, only layers or faults with offsets greater than ¼λ can be resolved by seismic reflection surveys. A peak frequency of 60 Hz from the air gun source used in the seismic reflection survey conducted in the Woodlark Basin can be assumed. A 60 Hz wave traveling through sediment with a seismic velocity of 1500 m s^{-1} results in a λ of ~25 m. Thus, any layer with a thickness less than ~6.25 m or any fault with an offset less than ~6.25 m will not be resolved (Figure 8). Using data from wells in the North Sea and extensive seismic reflection datasets, Walsh et al. (1991) estimated that unresolved extension comprises ~30 to 50% of total estimated extension. Based on the results of Walsh et al. (1991), Kington and Goodliffe (2008) assumed that unresolved faults account for 50% of the total extension and concluded that 34 km

of additional extension should be added to that estimated from seismic reflection data.

Figure 8. Faults observed in outcrop in the Gulf of Corinth, Greece. Offsets of this scale would not be resolved in a typical crustal scale seismic reflection study. Photo courtesy of Andrew Goodliffe.

Reston (2005) examined the impact of polyphase faulting using seismic reflection data from the Galacia Bank and the Vøring Sea. As extension on a fault increases, the fault will rotate towards a lower angle, failing at approximately 35° due to gravitational forces that increase the coefficient of friction along the fault. Once the original fault has locked, new faults may start forming to accommodate the strain, which nucleate at 65-70° and may cross-cut older faults. The original phase of faulting can be difficult to interpret in seismic reflection data and under extreme circumstances may be mistaken for stratigraphy. Reston (2005) estimated that polyphase faulting becomes important if extension has more than doubled the basin width. Kington and Goodliffe (2008) proposed two phases of faulting in the Woodlark Basin (Figure 9) based on an

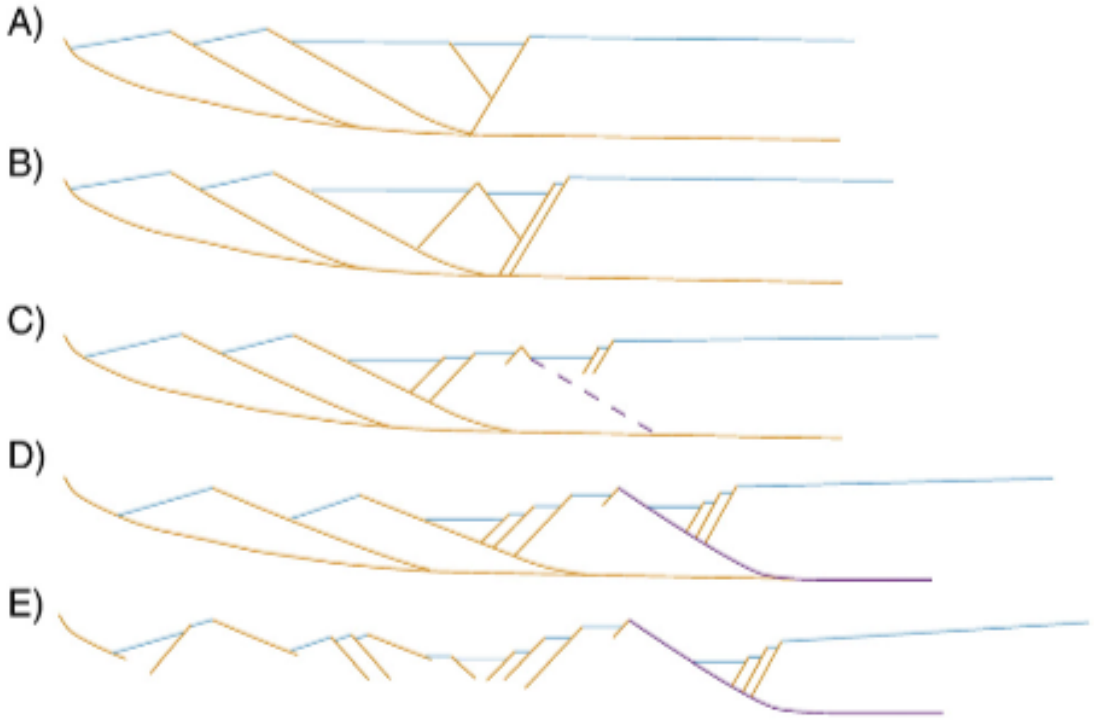

Figure 9. Polyphase fault model from Kington and Goodliffe (2008). In panel E, a new phase of faulting is observed. This cross-cuts the faults developed in panels A through D.

evolutionary model developed for rifting in the basin. Rifting from the first phase added ~20 km of extension to estimates along their profile.

An additional source of error not previously incorporated by Kington and Goodliffe (2008) is unrecognized metamorphic core complexes, which can lead to an underestimate of extension due to the great amount of strain involved in exhumation. Martinez et al. (2001) proposed that metamorphic core complex exhumation is accomplished by density inversion, and the width of the core complex can provide an estimate of extension. Lister and Davis (1989) interpreted exhumation as occurring along a low-angle detachment fault, where the entire heave of the detachment would give an approximation of extension (Figure 10). In either case, if a metamorphic core complex were to undergo a subsequent phase of brittle faulting, the exhumation history may be masked. This study reviews the impact of these potential sources of error to extension estimates in the Woodlark Basin. A primary goal is determining if the methods employed by Kington and Goodliffe (2008) can produce results that are precise and accurate enough to support their depth-dependent extension model.

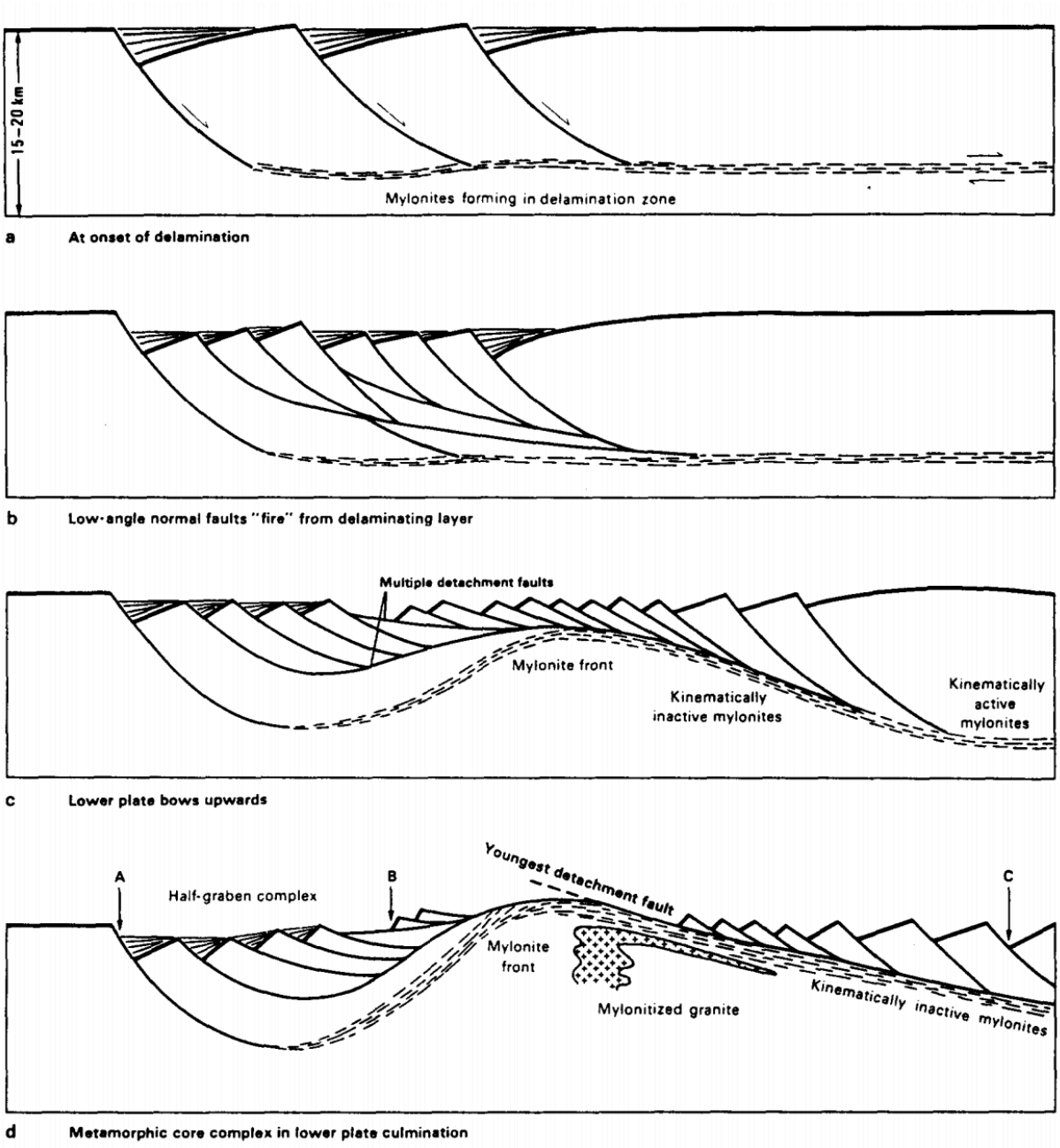

Figure 10. Model for the formation of a metamorphic core complex from Lister and Davis (1989).

CHAPTER 3: METHODS

3.1: Data

The data used in the current study include compilations of bathymetry, seismic reflection, magnetic data, and topography gathered during research cruises on the R/V *Maurice Ewing* and the R/V *Moana Wave* (Goodliffe et al., 1999). Seismic reflection data were collected using an air gun source and a two-fold 100 m long streamer with 6 channels on the R/V *Moana Wave*. North-south seismic reflection lines that were collected every 5 nautical miles between 152°E and 153°E are examined (Figure 11; Goodliffe et al., 1999). Bathymetric data were collected using interferometric and multibeam surveys (Goodliffe et al., 1999). Magnetic data were collected using a proton precession magnetometer on both cruises.

3.2: Extension from Brittle Faulting

Seismic reflection data along lines 100, 140, 150, 160, 180, 190, and 200 (Figure 11) were interpreted using Petrel. Lines 110, 130, 170 and 210 could not be used due to their poor quality. Bathymetric data were used to guide fault interpretations along each seismic reflection line. The basement reflector was interpreted to be the base of the syn-rift sediments, similar to that observed in ODP Leg 180 results to the west of the study area at 151.35°E (Taylor and Huchon, 2002). No coherent reflectors were observable below the basement reflector. High amplitude reflectors at the top of a section with stratified seismic character (alternating positive and negative high amplitude horizontal reflectors) were picked as horizons. Offsets on these

horizons are along faults dipping between 30 and 60°.

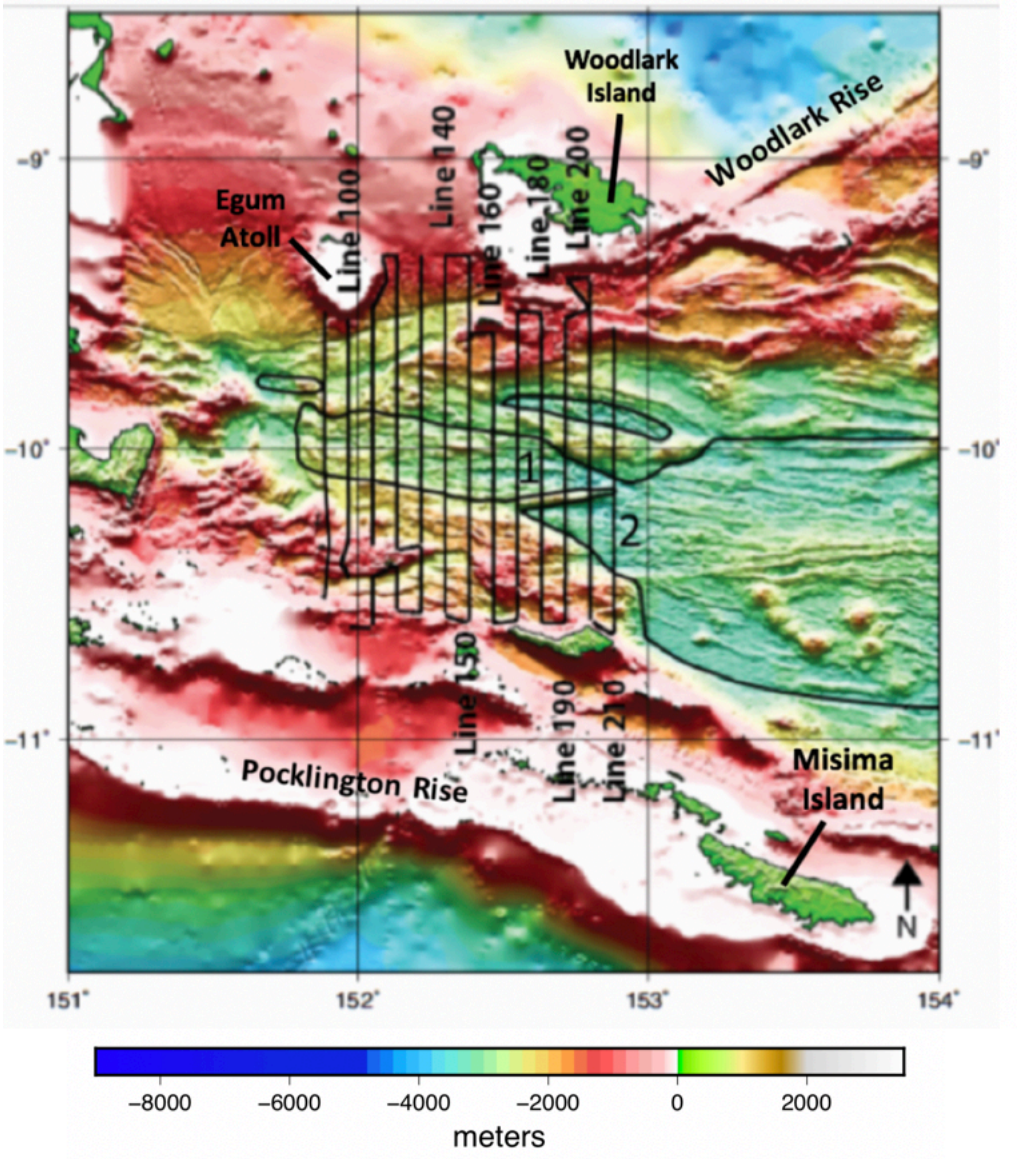

Figure 11. Bathymetry and seismic reflection survey lines in the Woodlark Basin. The continent-ocean boundary is outlined in black. The color scale (bottom) indicates relief in meters. Seismic reflection lines 90 to 210 are shown in black. Lines used for this study are labeled. Spreading segments are numbered based on Taylor et al. (1999).

The horizontal offset of each normal fault (heave) was measured and summed to derive extension estimates along each seismic reflection line. Figure 12 shows an example of this method along line 100. At the southernmost portion of the seismic line, three large continental blocks, separated by normal faults dipping at ~40°S and spanning 26 km, are evident (Figure 12).

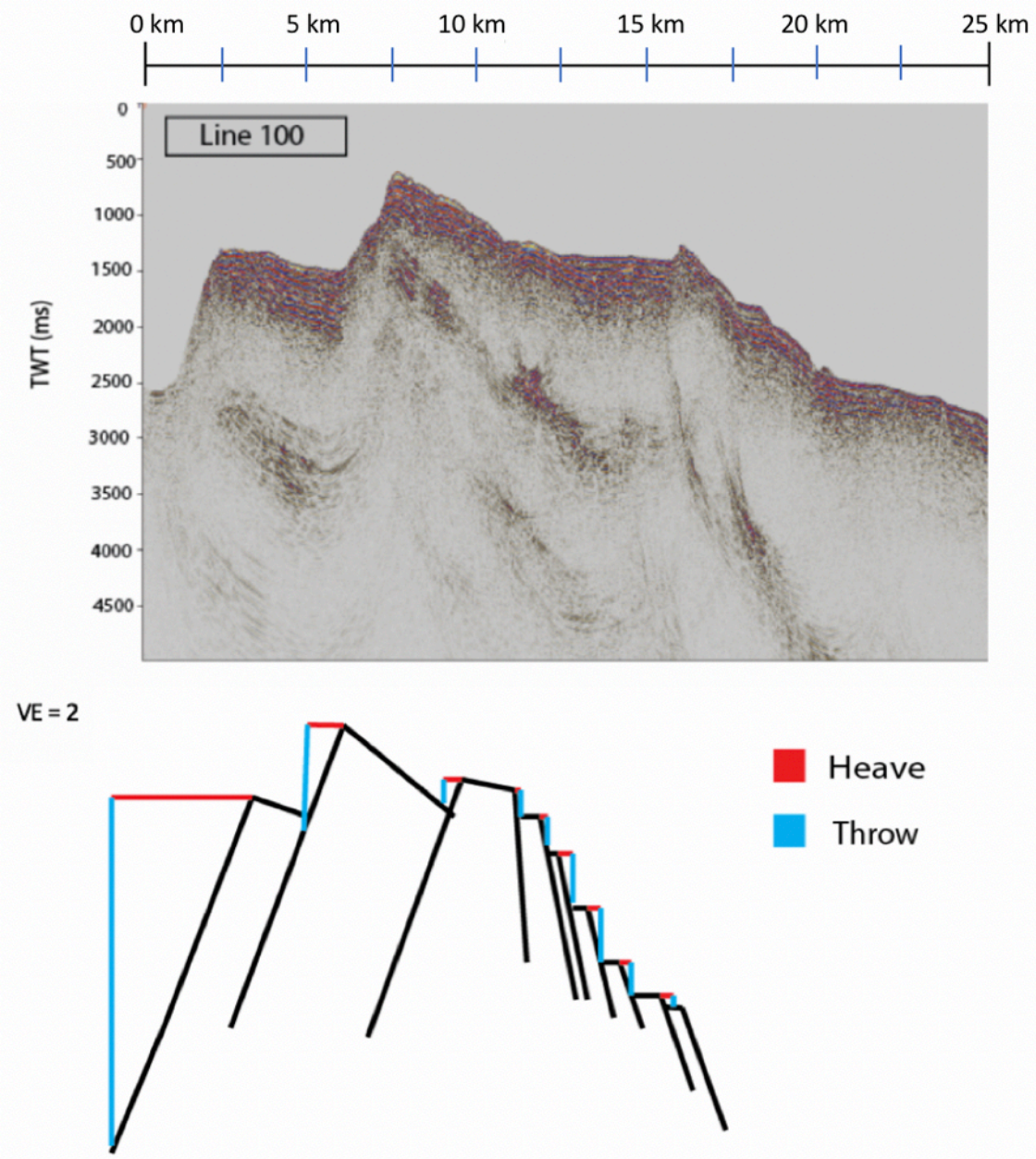

Figure 12. Offsets of normal faults based on seismic reflection line 100. The horizontal component of extension is the fault heave. Heaves were summed to estimate total extension.

Heaves range from 1.3 to 1.5 km. The northernmost of these blocks is faulted on the northern side facing the continent-ocean boundary. These faults occur every 1 to 1.5 km and dip at ~25°N to ~35°N with heaves that range from 0.2 to 0.3 km. Oceanic lithosphere was identified on the basis of an extremely chaotic and rough seismic character along the basement reflector. Magnetization chron data and the continent-ocean boundary from Taylor et al. (1999) were used to confirm the location of the oceanic lithosphere (Figure 13). As fault locations were determined by offsets in the bathymetry, error bars for the visible fault offsets were calculated based on the

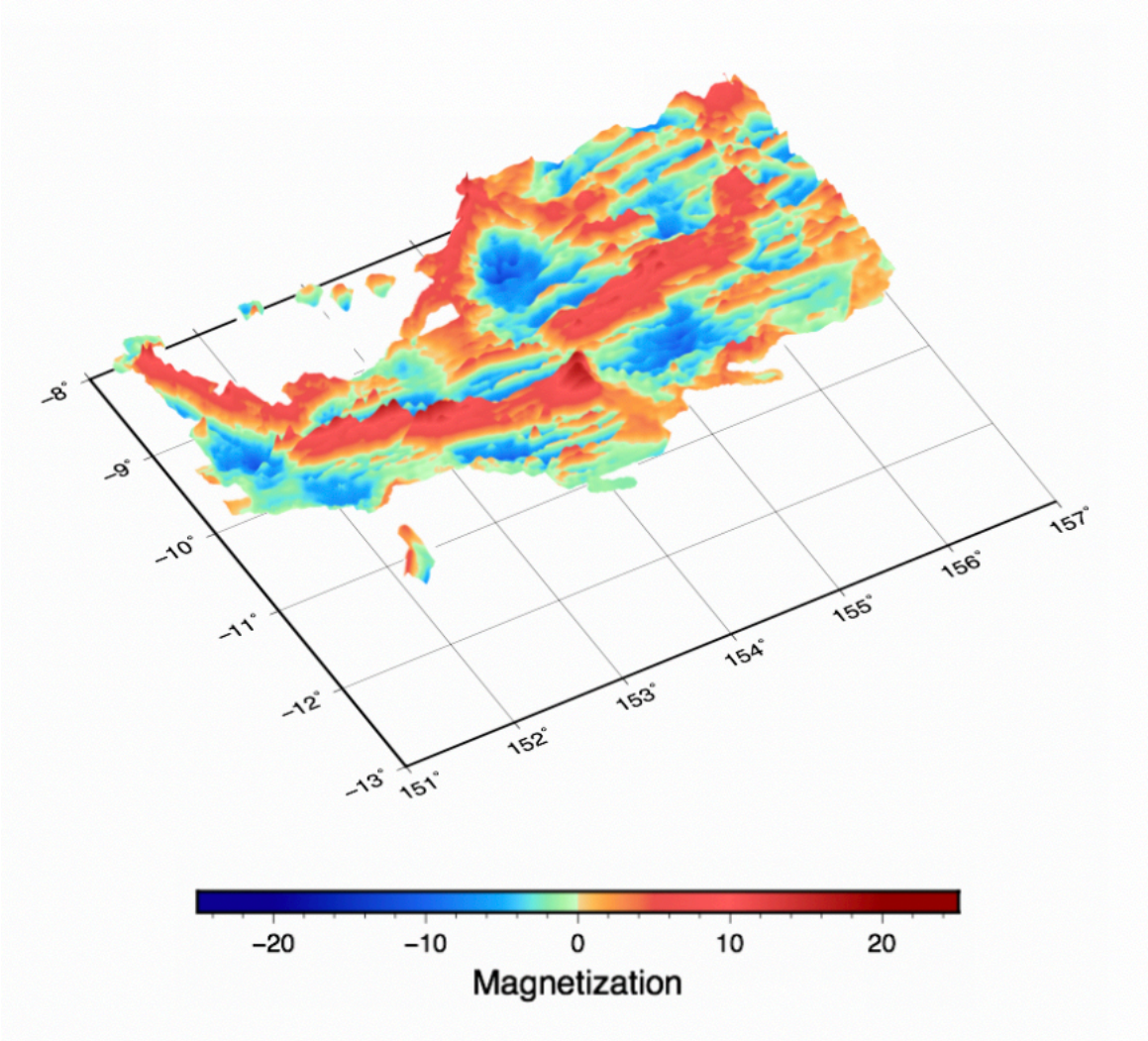

Figure 13. Seafloor magnetization map of the Woodlark Basin from Taylor et al. (1999). Positive magnetization is shown as positive relief in red. Negative magnetization is shown in blue. The lineations on the map correspond to magnetic isochrons.

bathymetry, which has a data pixel size of 200 m. With this resolution, the surface expression of a fault cannot be resolved horizontally below 400 m.

To account for subseismic faulting, extension calculated from fault heaves was increased 50% based on the methodology of Walsh (1991) and Kington and Goodliffe (2008) to provide an estimate of maximum brittle extension. A polyphase faulting model, assuming two phases of faulting, was developed in order to get an estimate of extension due to the first phase of faulting in the basin (Figure 14). Seismic reflection line 100 was chosen for interpretation because it shows rifted continent separated by only one spreading center. In addition, this profile has the

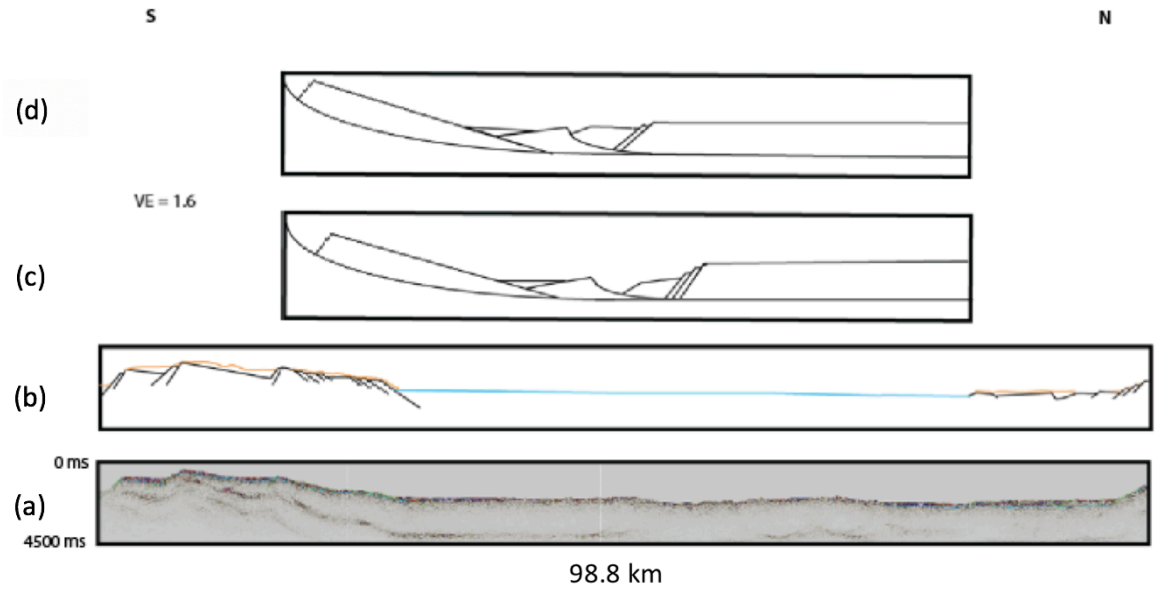

Figure 14. Polyphase faulting model. (a) Seismic reflection along line MW9304-100. (b) Illustration based on the interpretation of the seismic line; oceanic crust is shown in blue, sediment is shown in orange. (c) After the current phase of faulting and oceanic lithosphere was removed, the cross-section was rebalanced. Large fault blocks suggest crustal scale detachment faulting as well as faults at low angles. (d) The smaller faults were interpreted to have initiated at higher angles and rotated along detachment faults.

most easily imaged basement compared to the other seismic reflection lines (Figure 14). This line will allow for a model with minimal impact due to rotation of faults during seafloor spreading and sedimentation. Rotation of faults during seafloor spreading can significantly

impact extension estimates close to continental margins. The most recent phase of faulting was interpreted to be on faults formed between 30° and 60°. The cross section was returned to its geometry prior to the initiation of seafloor spreading and the newest phase of faulting. Moresby Seamount spans ~20 km north to south within the Kington and Goodliffe (2008) study area and is proposed to be fault controlled (Figure 3). Although there is little evidence of this seamount along seismic line 100, there is a ~10 km ridge at the northern end of the line. This ridge is more pronounced in seismic reflection lines 140-200. The seamount is interpreted in the polyphase model (Figure 14) as being faulted many times and incorporated into the largely subsidence-controlled northern margin as rifting progressed.

The first phase of faulting is interpreted to have initiated at a higher angle that later rotated to a lower angle. In the southern portion of the cross-section, two large continental blocks are observed, separated by faults dipping at ~20°N (Figure 14). Goodliffe and Taylor (2007) indicate that faults in the basin fail at lower angles due to fault zone serpentinization in Papuan Ultramafic Belt rocks. The fault heaves of the interpreted first phase of faulting in the polyphase model were added to the overall total. Fault blocks observed along lines 140 and 200 that have a similar geometry to line 100 (~20° to 30° dip) are interpreted to be remnants bounded by extinct rotated faults. The first phase of extension on these faults is summed to obtain total extension estimates for each line. Similar geometries are not imaged on lines 150, 160, 180, and 190. The polyphase extension estimate from line 140 was used for lines 150 and 160 based on their proximity and similar bathymetric profile. East of line 160, there is more than one spreading center along the profile. Therefore, for lines 180 and 190, the sum of the polyphase extension estimate from line 200 is used.

3.3: Extension from Subsidence

McKenzie (1978) described a method to estimate extension from subsidence. Parameters include the densities of the different rock and sediment layers, the sedimentary basin thickness, and the crustal and lithospheric thicknesses. Thermal properties, including the temperature at the Earth's surface and the top of the asthenosphere, and the expansion coefficient of the mantle are also needed. The relationship between extension and subsidence was further developed by Turcotte and Schubert (2002). Additional assumptions included instantaneous rifting, Airy isostasy, and an average geothermal gradient consistent with the continental lithosphere. Extension is removed by assuming constant area and reconstructing the crustal volume to an isostatically balanced rectangle in cross-section.

The crustal thinning factor (β) along each rift basin profile was calculated using Equation 2. Basin thickness (*hsb*) was obtained from seismic reflection and bathymetry data. Bathymetry used for the calculation follows the north-south profiles, extending beyond the end of each seismic line (Figure 11).

$$\beta = \left(1 - \frac{hsb}{\left(\frac{\rho_m - \rho_{cc}}{\rho_m - \rho_s}\right)(h_{cc}) - \left(\frac{1}{1.16\sqrt{\pi}}\right)\frac{(p_m \alpha_v (T_1 - T_o) l_{cc})}{(\rho_m - \rho_s)}}\right)^{-1} \qquad (2)$$

Kington and Goodliffe (2008) assumed the following parameters: mantle density (ρ_m) = 3300 kg m^{-3}; crustal density, including incorporation of ultramafic rocks from the Papuan Ultramafic belt (ρ_{cc}) = 2800 kg m^{-3}; pre-rift crustal thickness (h_{cc}) = 35 km, based on receiver functions (Abers et al., 2002) and a refraction study from Abers et al. (1997); pre-rift lithospheric thickness (l_{cc}) = 160 km (Kington and Goodliffe, 2008), based on the depth to the 1300˚C isotherm at the base of the lithosphere; sediment density (ρ_s) = 1500 kg m^{-3}; and surface

temperature (T_o) = 300.15 K. A thermal expansion coefficient for the mantle with forsterite composition (α_V) = 3.28 x 10^{-5} K^{-1} was also assumed. These values were applied for the current study. Error estimates were determined based on the maximum and minimum extension estimates possible for a combination of all assumptions; errors will be discussed in the results.

The first portion of the denominator (Equation 2) relates to the density ratio of the mantle, crust, and sediments in the basin. The second portion of the denominator relates to the thermal properties and their effects on the expansion of the mantle during subsidence. A shortcoming of Equation 2 is the assumption of Airy isostasy. Rift basins tend to behave with some rigidity due to their lateral strength and elastic thickness (Davis and Kuznir, 2004). Assuming no flexural rigidity in the basin results in an underestimate of extension. Additionally, assuming that subsidence began at sea level will underestimate extension if there was initially topography during rifting.

Determining β (Equation 2) allowed for calculation of the approximate thickness of the stretched continental crust (s_{cc}). The total area of continental crust was determined from the calculated stretched crustal thickness (s_{cc}) and the current basin width (w_o). The upper surface of each crustal profile was returned to sea level and the Moho to a depth of 35 km. As area would need to be maintained, using the assumed initial crustal thickness (h_{cc}) and the calculated total area of the basin allowed the initial basin width (W_i) to be determined (Equation 3). The final basin width (w_o) minus the initial basin width (W_i) gives the amount of extension from subsidence.

$$W_i = \frac{s_{cc} * w_o}{h_{cc}} \qquad (3)$$

The seismic reflection lines do not extend to the margin edges (Figure 11). Beyond the ends of the seismic reflection lines, extension as predicted by subsidence was used and added to the extension derived from brittle faulting.

3.4: Extension from Euler Pole Kinematics

Euler pole derived opening rates for the Woodlark basin assume a two-plate solution (Taylor et al., 1999) with a 95% confidence interval regarding the location of the Euler poles. Using the results of Taylor et al. (1999), the width of the oceanic lithosphere between 152°E and 153°E (Figure 11) was determined (Figure 15). This estimate was subtracted from the total predicted extension to determine the predicted continental extension along each line.

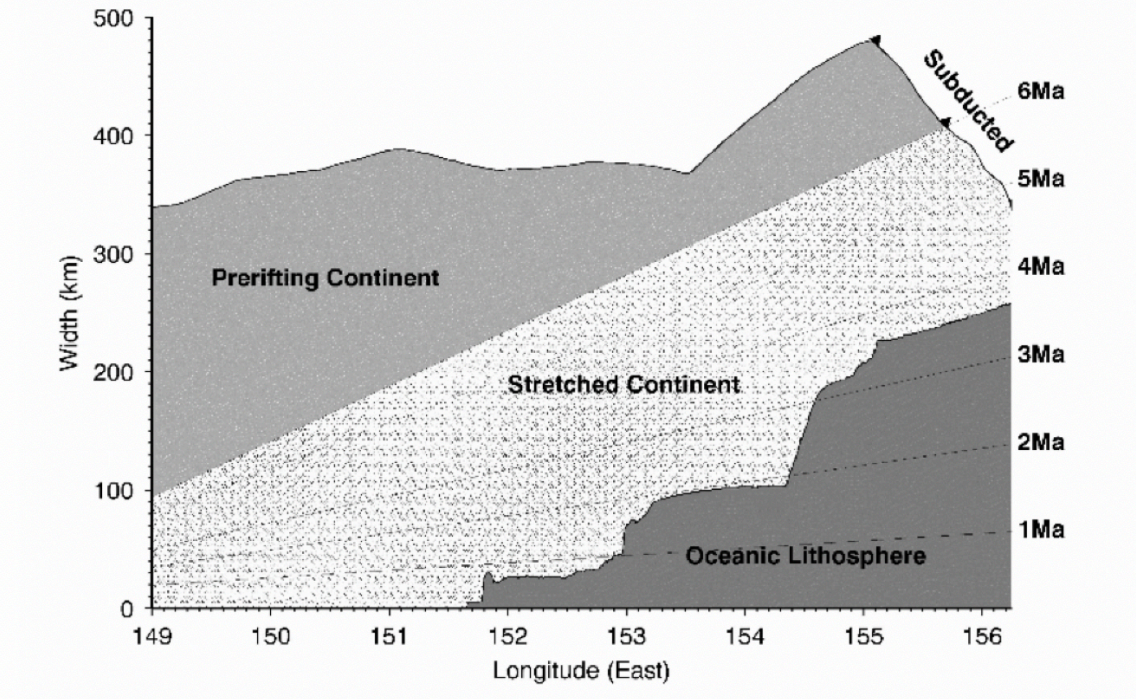

Figure 15. Plot of cumulative continental and oceanic widths of the Woodlark Basin versus longitude (from Taylor et al., 1999). The diagonal isochrons, labeled in Ma, are derived from the best fitting poles of opening and are dashed where extrapolated from 1 to 6 Ma. Total opening is partitioned between continental stretching and seafloor spreading. The width of continental lithosphere includes calculated pre-rifting and stretched components.

CHAPTER 4: RESULTS

4.1: Brittle Extension Estimates

Line 180 is used as a representative example to describe the results as it contains two spreading centers as well as thick syn-rift sediment packages (0.2 to 0.6 km thick). The interpretations of seismic lines 100, 140-160, and 190-200 are discussed in Appendix A. For each seismic line, basin depths were calculated using a velocity of 1500 m s^{-1}, which is the approximate velocity of unconsolidated sediments. The strike of faults was determined from bathymetry.

Starting at the southernmost portion of line 180 (at 0 km, Figure 16), there is a 5 km wide continental block with a minimum water depth of ~1.4 km; it is cut by four normal faults with heaves ranging from 0.1 to 0.2 km and dipping ~40°N. The faults are covered by sediment that is ~0.4 km thick. A structure interpreted as a small horst is evident at 30 km (Figure 16); it is separated from the large continental block by a normal fault with a heave of 0.2 km dipping at ~45°S. The horst reaches a minimum water depth of ~1.8 km and spans a distance of 1.2 km; a normal fault with a heave of 0.6 km dips ~45°N and forms the northern boundary. On the northern side of the horst, three faults dipping ~30°N down-step from ~1.4 to ~2.1 km water depth and span a distance of 8 km; heaves range from 0.8 to 1.2 km. The fault blocks are covered with ~0.2 km of sediment. To the north (at 39 km, Figure 16), another horst is evident with water depth decreasing to ~1.7 km. The horst spans a distance of 0.8 km. It is formed by a fault on the southern side dipping ~40°S with a heave of 1 km. On the northern side at 40 km, a fault with a

heave of 1.5 km dips ~40°S, separating the horst from a graben, reaching a water depth of ~2 km (Figure 16). The graben spans a distance of 2.7 km; it is separated from another horst, spanning a distance of 1.3 km and reaching a minimum water depth of 1.7 km, by a fault dipping ~50°N

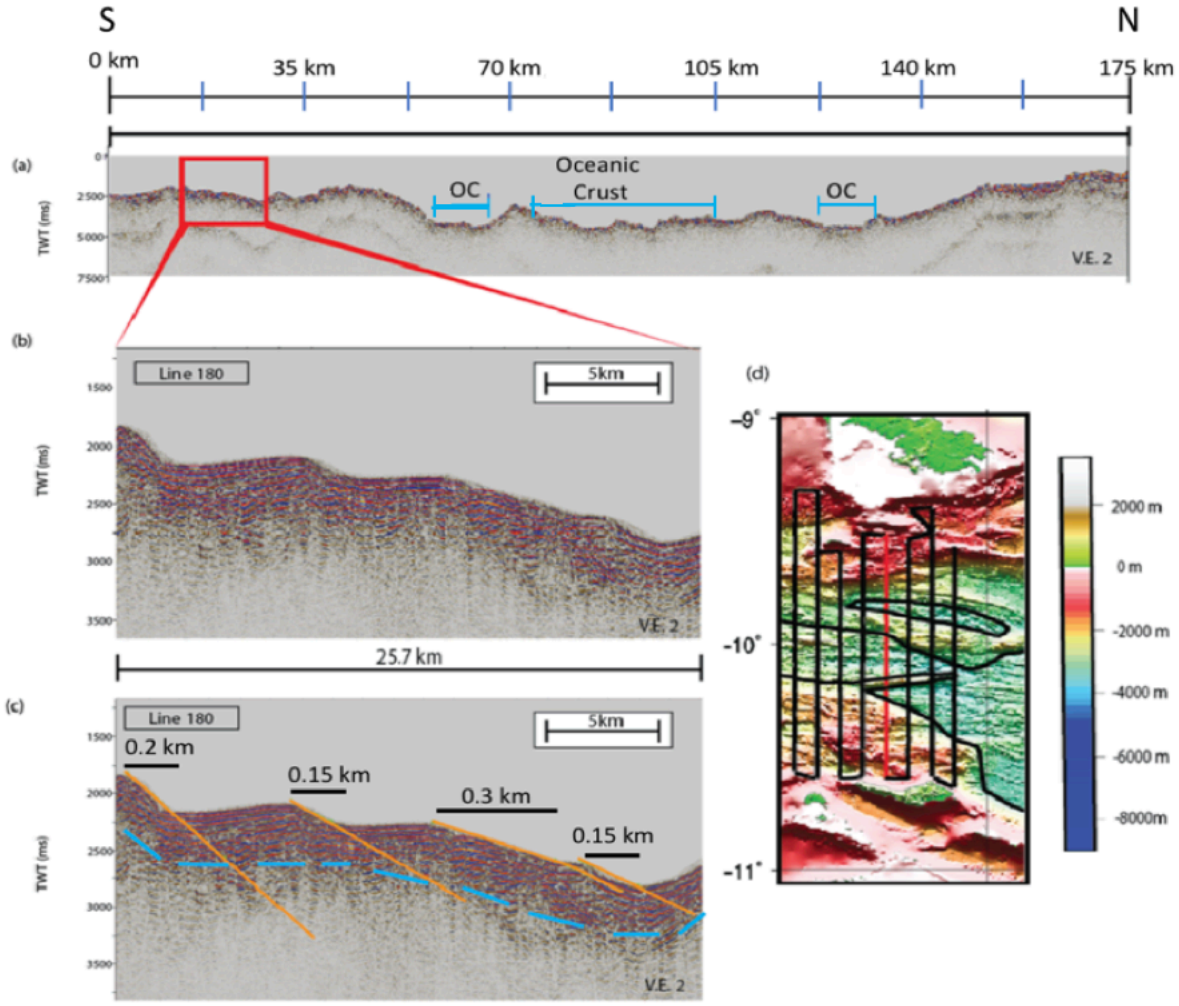

Figure 16. (a) Seismic Line MW9304-180. Vertical exaggeration is 2. The red box indicates the location of the detailed section (b and c) on the northern end of the profile. The extent of oceanic crust (OC) is shown by the solid blue line. The map in (d) shows the location of the seismic reflection line (highlighted in red). (b) Uninterpreted and (c) interpreted seismic reflection data. Faults are shown by the orange lines. The basement reflector is annotated by a dashed blue line.

with a heave of 0.4 km (at 43 km, Figure 16). No sediment is evident on the horsts; however, the graben contains a sediment package ~0.5 km thick. To the north of the horst at 45 km (Figure 16), a series of 13 faults exist that down-step from a water depth of ~1.3 to ~3.2 km and continue

to the continent-ocean boundary over a distance of 12 km. The normal faults dip ~45°N, with heaves ranging from 0.4 to 0.8 km.

At 57 km, a fault separates the continental block from the southern continent-ocean boundary with a heave of 1.7 km (Figure 17). Oceanic crust (segment 2; Figure 3) extends for 6 km to the north and is characterized by a rough basement texture. The maximum water depth is ~3.3 km. To the north of the oceanic lithosphere, there is an isolated continent block that is 10.5 km wide (Figure 17). A ~0.5 km thick sediment package tops the continental block. Water depths decrease to the north of the continent-ocean boundary from ~3.3 to ~2.3 km over a lateral distance of 3.1 km. Three large faults that dip at ~45°S and up-step to the north are evident on the southern side of this continental block. Heaves range from 0.4 to 0.7 km. On the northern side of the block, at 76 km, additional faults with heaves ranging from 0.1 to 0.3 km down-step to the continent-ocean boundary to the north (Figure 17). Water depths increase from ~2.3 to ~3.3 km over a lateral distance of 7.4 km. Oceanic crust (segment 1; Figure 3) is present for 30 km to the north with a maximum water depth of ~3.3 km. At 105 km, another isolated continental block spans a distance of 18 km, reaches a minimum water depth of ~2.6 km, and is separated from the oceanic crust by a normal fault with a heave of 0.2 km dipping at ~50°S (Figure 17). Another fault with a heave of 0.3 km occurs to the north, also dipping at ~50°S. To the north of this fault, there are large horst and graben structures at 105 to 122 km (Figure 17). The structures are separated by normal faults dipping at ~40°N and 40°S with heaves ranging from 0.5 to 0.7 km. There is ~0.5 km of sediment infill in the grabens. On the northern side of the continent block, there are three faults that down-step to the north from a depth of ~2.5 to ~3.3 km. The faults dip at 30°N as they approach another continent-ocean boundary. The heaves of these faults range from 0.6 to 0.7 km. Continuing to the north, oceanic lithosphere outcrops on

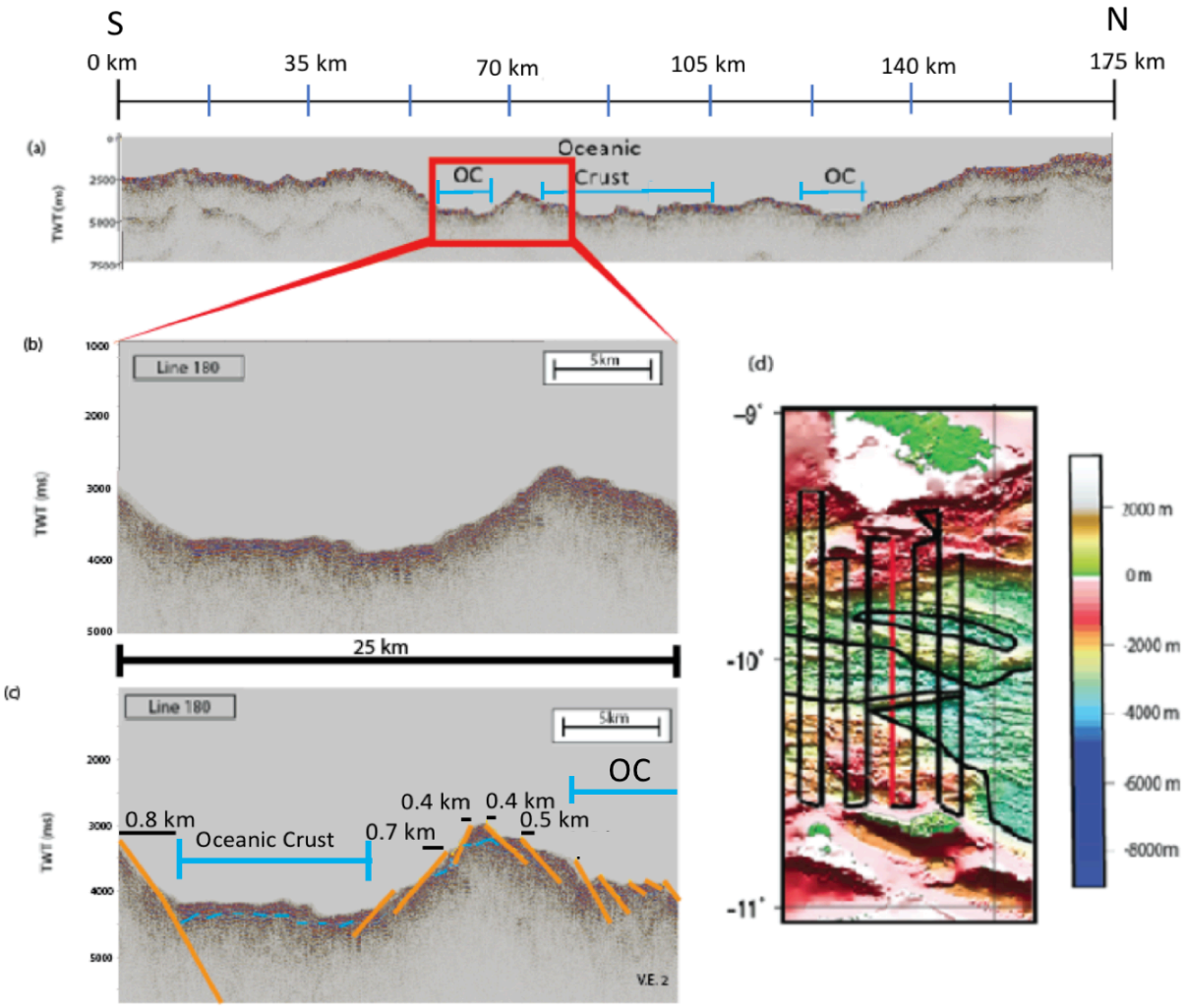

Figure 17. Same as Figure 16 but for a section in the middle of seismic line MW9304-180.

the seafloor over a distance of 4 km between 122 and 126 km (Figure 17); the maximum water depth remains constant at ~3.3 km. The northern continental margin is separated from the oceanic lithosphere by a normal fault dipping at ~50°S with a heave of 0.5 km. Normal faults dipping ~45°S along the continental block up-step to the north from a water depth of ~3.3 to ~1.2 km over a distance of 14 km. The fault heaves range from 0.1 to 0.5 km. At 140 km, a normal fault dipping at ~50°S with a heave of 0.3 km begins a series of faults down-stepping to the north (Figure 17).

A ~0.6 km thick sediment package overlays the northern portion of the seismic line, making the heave and exact angle of the faults harder to interpret (Figure 18). Two normal faults dipping at ~30°S and down-stepping to the north are evident below the sediment package. There was no offset on these faults at the surface due to the horizontally deposited sediment cover. However, the sediment onlaps onto the ~30°S dipping faults at depth, which indicates these fault are growth faults and the sediments were deposited synrift. Growth faults such as this are seen on almost all other seismic lines. The heave at depth is ~0.9 km. The northernmost fault forms the northern portion of a graben, spanning a distance of 3.3 km with a water depth of 1.2 km, which is separated from another up-thrown block (~0.8 km water depth) to the north by a fault with a heave of 0.2 km dipping ~45°S. The up-thrown block contains three faults dipping ~45°S, up-stepping from water depths of ~0.8 to ~0.7 km over a distance of 3.1 km. Heaves of 0.4 to 0.5 km are evident despite the ~0.5 km thick sediment cover. At 166 km, an asymmetric graben, 1 km wide with a maximum water depth of 1.2 km, is filled with 0.5 km of sediment; it is bounded by a fault dipping ~35°N on the northern side and another fault dipping ~45°S on the southern side (Figure 18). The latter fault has a heave of 0.3 km and separates the graben from a horst that is 0.2 km wide with a water depth of ~0.7 km to the north. At 170 km, on the northern side of the horst (Figure 18), a fault dipping ~35°S has a heave of 0.1 km. Sediment cover is ~0.3 km thick and masks the remaining 2.3 km of the seismic line.

All observable fault heaves from line 180 were summed, giving a brittle faulting extension estimate of 30.5 km. For lines 100, 140-160, and 190-200, the process was repeated (Table 1). As noted before, the bathymetry data pixel size of 200 m makes it so the surface expression of a fault cannot be resolved horizontally better than 400 m. Therefore, as seismic

reflection line 180 has 68 interpreted faults, error estimates are ±27 km for the entire line. The

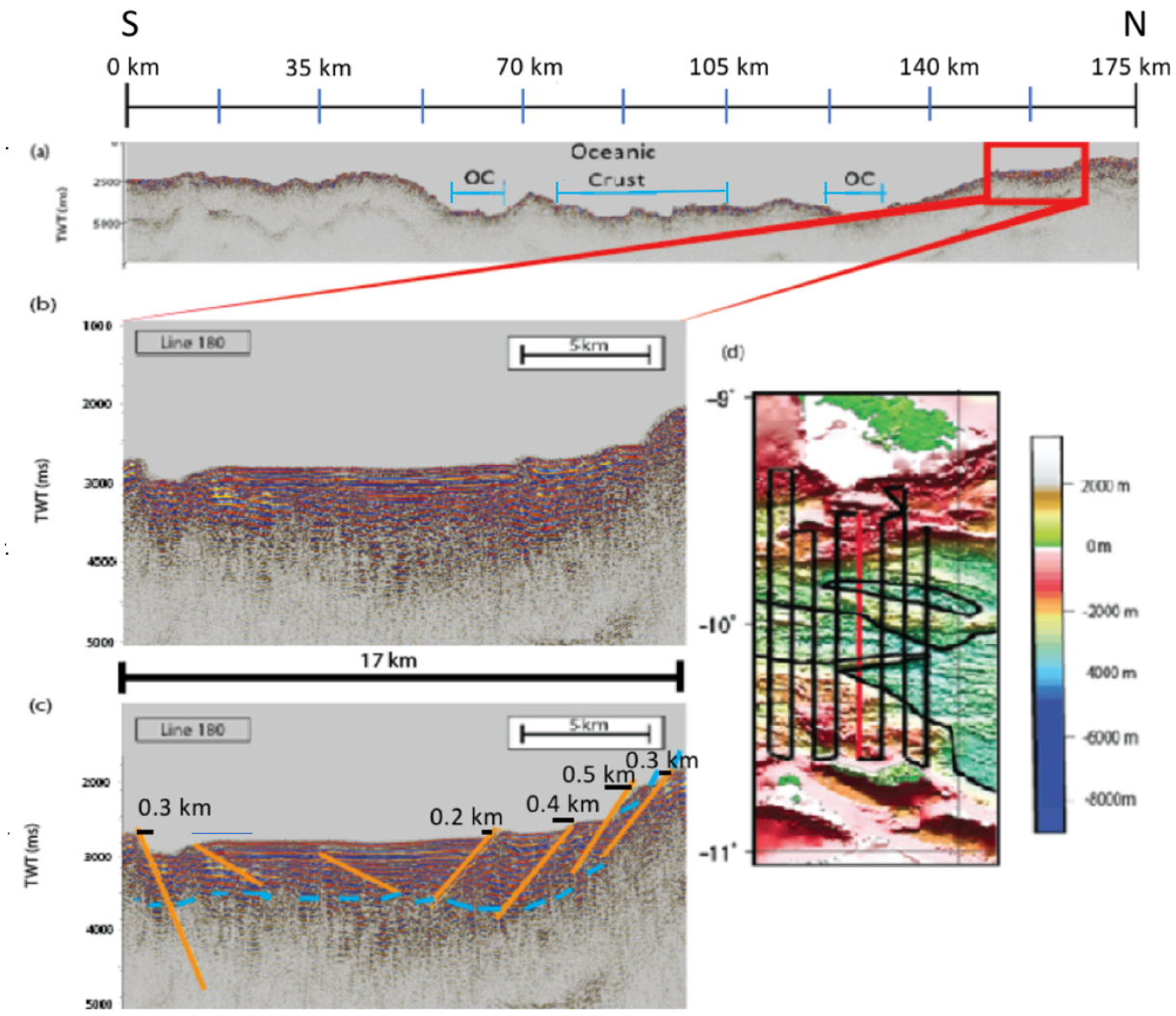

Figure 18. Same as Figure 16 but for a section at the southern end of seismic line MW9304-180.

same method was used for error estimates along other interpreted seismic lines (Table 1). The average number of faults interpreted for each line was 69, excluding the shorter line 100 that contained only 25 faults. Based on (Walsh, 1992), subseismic resolution faulting was estimated by assuming that unresolved faults account for an additional 50% of the total extension. This gives an upper-end estimate of unresolved extension of ~15 km for line 180. Table 1 shows the estimates for the other lines.

Again, the polyphase fault model is based on line 100. For the other lines, similar geometries to those observed on line 100 were interpreted to have formed from a similar polyphase process. The summation of the heaves resulting from the first phase of faulting added ~25 km of extension for line 100. Similarly, ~28 km of extension was added for lines 140-160, and ~26 km of extension was added for lines 180-200 (Table 1). Extension along the portions of the lines outside the seismic coverage area (Figure 11), based on the subsidence method (Section 3.3), added 26 km (+22, -14) of extension to line 180. The total extension estimated along line 180 is 84.3 km (+46, -33), corresponding to a β of 1.51 (+0.56, -0.25). Error estimates for β are determined based on the maximum and minimum sources of error to the brittle extension estimate. The remaining seismic lines were interpreted using the same methods as those applied to line 180 (Table 1). β values range from 1.31 to 1.57. The average error for estimates of extension from brittle faulting is +19 km, -9 km.

Table 1. *Brittle extension estimates for seismic lines MW9304-100, 140, 150, 160, 180, 190, and 200.*

	Brittle Extension from Fault Heaves (km)	Extension from Subresolution Faulting (km)	Polyphase Extension Estimate (km)	Extension Where There is No Seismic Coverage (km)	Total Extension (km)	Extension Factor
Line 100	11.6 (±10)	5.8	~25	26 (+22, -14)	68.5 (+32, -24)	1.37 (+0.29, -0.16)
Line 140	24.5 (±17)	12.25	~28	14 (+14, -8)	78.8 (+31, -25)	1.53 (+0.40, -0.22)
Line 150	26.8 (±19)	13.4	~28	24 (+20, -13)	92.1 (+39, -32)	1.57 (+0.51, -0.26)
Line 160	28.3 (±22)	14.15	~28	20 (+ 20, -9)	90.4 (+42, -31)	1.56 (+0.53, -0.25)
Line 180	30.5 (±27)	15.25	~26	12 (+19, -6)	84.3 (+46, -33)	1.51 (+0.56, -0.25)
Line 190	30.9 (±21)	15.45	~26	13 (+20, -7)	84.3 (+41, -28)	1.51 (+0.48, -0.21)
Line 200	28.2 (±23)	14.1	~26	10 (+19, -5)	76.2 (+42, -28)	1.41 (+0.40, -0.16)

4.2: Extension Estimates from Subsidence

The bathymetry along line 180 is plotted to show seafloor as a function of latitude between 8.75°S and 11.26°S (Figure 19). Using the assumption of Airy isostasy, bathymetry allows for the calculation of Moho depth (Equation 2). These estimates, corrected for thermal effects along the seismic line, are plotted as a function of latitude to illustrate how crustal

thickness changes based on the depth of the sedimentary basin (Figure 19). This process is repeated for lines 100, 140-160, and 190-200 (Appendix B).

Over the Pocklington Rise, the water depth decreases to 5 m; crustal thickness is ~35 km. To the north of the rise, a large graben reaches a maximum water depth of 1.8 km, and the thickness of the crust is 25 km. Line 180 crosses over Misima Island to the north of this graben, where crustal thickness reaches ~36 km, and topography reaches 0.5 km above sea level. Water depth increases to 1.5 km on the northern side of Misima Island. A series of horsts and grabens have varying water depths (1 to 2 km) approaching the southern continent-ocean boundary. A maximum water depth of 3.2 km is occurs over the oceanic lithosphere (spreading segment 2), and the thickness of the oceanic crust is ~10 km. A continental fault block separates spreading segment 2 from spreading segment 1. The block reaches a minimum water depth of 1.4 km; crustal thickness is 14 km. Spreading segment 1 has a maximum water depth of 3.4 km and a crustal thickness of 10 km. Another continental fault block is directly to the north of spreading segment 1. Here, a minimum water depth of 2.5 km is reached, and the continental crust is 1.5

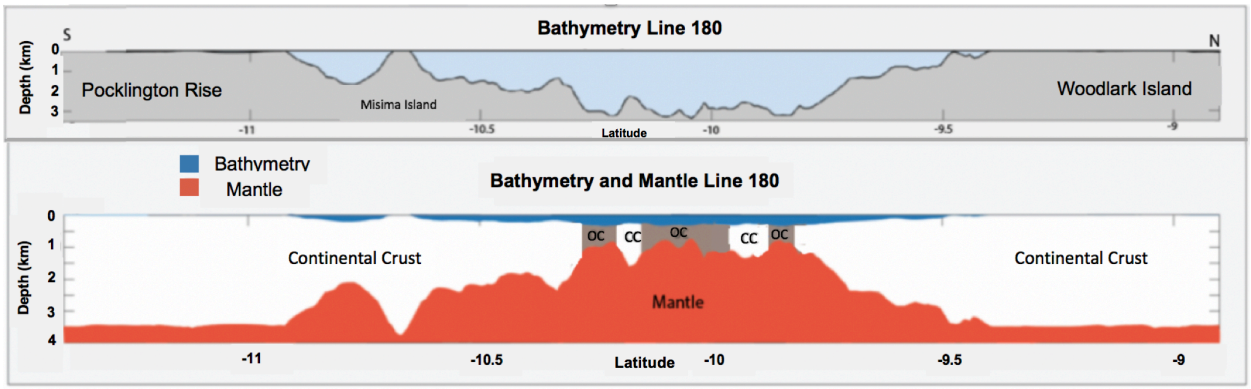

Figure 19. Crustal profile along seismic reflection line 180. (a) Bathymetry plotted as a function of latitude. b) Bathymetry (blue) and calculated depth to Moho (red) plotted as a function of latitude. Continental crust is shaded white. Oceanic crust is shaded dark grey.

km thick. To the north, another segment of oceanic lithosphere is present, with a maximum water depth of 3.2 km and a 10 km thick crust. The water depth decreases 2.5 km approaching the

continent-ocean boundary. To the north of the boundary, continental crust thickens to 35 km. Woodlark Island reaches heights of 63 m above sea level. To the north of the island, the water depth increases to 57 m in the northernmost portion of the subsidence profile.

For calculations of subsidence, cross-sectional areas of oceanic crust and sediment thickness were ignored. For line 180, the water depth and the depth to the Moho give a crustal cross-sectional area of 6.7×10^6 km. Based on the assumption that the initial crustal thickness is 35 km (Abers et al., 2002; Kington and Goodliffe, 2008), the pre-extension basin width is 184 km (Equation 3). Current basin width, excluding oceanic crust, is 244 km, giving a total extension predicted from subsidence for line 180 of 60 km. To account for errors due to the assumptions in Equation 2, sediment thickness, initial crustal thickness, and density were tested by changing individual variables and determining how extension would be impacted for each line. As an example, for line 180, increasing sediment thickness from 0 to 0.5 km increases extension to 95 km (+32, -40). Decreasing the continental crust density from 2800 to 2750 kg m^{-3} decreases extension to 48 km (+ 27, -24). Increasing the initial crustal thickness from 35 to 50 km decreases extension to 28 km (+16, -4). Based on maximum and minimum possible sources of error for an extreme scenario, error bars of (+35 km, -34 km) are assigned to the overall estimate of extension (60 km, Table 2). This value is equivalent to an extension factor of 1.31 (+0.29, -0.19). Errors limits are determined for lines 100-140, 150-160, and 190-200 using the same method employed for line 180. The total extension estimates and extension factors for each line are summarized in Table 2. A maximum extension factor of 1.51 (+0.37, -0.39) was obtained for line 140. The extension factor decreases to 1.31 (+0.29, -0.19) at line 180 and then increases to 1.41 (+0.33, -0.27) at line 200. The average error for estimates of extension using subsidence is +34 km, -41 km.

Table 2. *Extension estimates from subsidence calculations*

	Total Extension (km)	Extension Factor
Line 100	68.15 (+33, -40)	1.37 (+0.3, -0.24)
Line 140	76.67 (+30, -52)	1.51 (+0.37, -0.39)
Line 150	71.75 (+33, -43)	1.39 (+0.32, -0.25)
Line 160	64.14 (+37, - 38)	1.33 (+0.33, -0.21)
Line 180	60.08 (+35, -34)	1.31 (+0.29, - 0.19)
Line 190	69.67 (+34, -40)	1.36 (+0.31, -0.22)
Line 200	79.25 (+36, -47)	1.41 (+0.33, -0.27)

4.3: Euler Pole Extension Estimates

Using the Euler pole derived extension results from Taylor et al. (1999) (Figure 15), the total extension and the extension factor is determined along each line (Table 3). Along line 180, there is 233 km of extension, 31 km of which is accommodated by accretion. This gives an extension factor of 3.03. Unlike the brittle faulting and subsidence results, extension rates determined from Euler poles consistently increase from west to east from 2.45 to 3.21. Euler poles are mapped in Figure 3 within 95% confidence intervals. Taylor et al. (1999) did not assign error bars associated with this confidence interval to their extension as determined through spreading rates (Figure 15).

Table 3. *Euler Pole Extension Estimates*

	Total Crustal Extension (km)	Extension Factor
Line 100	202	2.45
Line 140	223	2.86
Line 150	224	2.87
Line 160	230.5	2.96
Line 180	233	3.03
Line 190	238	3.18
Line 200	234	3.21

CHAPTER 5: DISCUSSION

5.1: Discussion of Results Based on the Methods of Kington and Goodliffe (2008)

Brittle faulting (average β of 1.49) and subsidence-derived (average β of 1.38) estimates of extension are consistent with each other within the error limits (+0.45, - 0.21 for brittle estimates; +0.36, -0.29 for subsidence estimates). This suggests that the previous extension discrepancy described by Davis and Kuznir (2004) can be partially explained by the inclusion of polyphase and subresolution faulting, as proposed by Kington and Goodliffe (2008). Extension estimates from Euler pole kinematics (average β of 2.98) are roughly double that of the subsidence and brittle faulting extension estimates. This is consistent with the results of Kington and Goodliffe (2008). Because estimates of extension derived from Euler poles and subsidence are both a measure of whole lithosphere extension, they should match if all parts of the lithosphere extend at the same rate. Kington and Goodliffe (2008) proposed that this remaining discrepancy between these two approaches can be explained by higher extension rates in the lower crust and lithospheric mantle prior to seafloor spreading. Because Euler pole derived extension factors are so much greater than the subsidence estimates, this indicates that either the brittle faulting or subsidence methods are flawed or that the Euler pole solutions are not correct for the Woodlark Basin. However, an alternative solution is that the error limits associated with subsidence and brittle faulting are potentially so great that evidence of depth-dependent extension cannot be resolved from the results. If this is the case, then the model proposed by Kington and Goodliffe (2008) is not warranted.

5.2: Potential Errors in Extension Estimates from Brittle Faulting

Several sources of error are not included in the brittle faulting estimates of Kington and Goodliffe (2008). These include a minimum estimate of the impact of subresolution faulting, the effect of sediment cover, and the possibility of an unrecognized metamorphic core complex. The current study uses the highest estimate of subresolution faulting (50%) recommended by Walsh (1991). If the minimum estimate (30%) were instead used, it would result in 9 km less extension along line 180. Thicker sediment cover could mask additional faults not recognized in this study. The extension due to a horizontally deposited 0.5 km thick sediment package in a graben at any water depth formed from a fault dipping at 30° can be estimated using the method shown in Figure 20. In this case, the sediment package would mask 0.86 km of heave. For seismic line 180 with 69 faults, this could mask up to 58 km of extension. An unrecognized metamorphic core complex could also lead to large underestimates in extension. The model of Martinez et al. (2001) predicted that the surface expression of a metamorphic core complex can be used as a measure of lateral extension. The N-S surface expression of the metamorphic core complex on Goodenough Island, which is one of the D'Entrecasteaux Islands, is ~40 km across. It is not unreasonable to assume that there are other unrecognized core complexes in the basin that have contributed to extension. However, to resolve the discrepancy between extension estimates following the model from Martinez et al. (2001), the core complex would need to be over ~100 km wide. Alternatively, based on Lister and Davis (1989), the width of a metamorphic core complex and the associated heave of the detachment fault that formed it is an estimate of total extension. For example, a detachment fault that formed at 30° and extended through the 35 km crust would have a heave of 60 km. Using the method of Lister and Davis (1989), the width of the Goodenough Island complex, in addition to the detachment fault that formed it, could

produce the 100 km of extension necessary to make estimates of extension from brittle faulting match that predicted by Euler pole kinematics. The presence of a foundered core complex in the vicinity of Misima Island has been proposed by Taylor and Huchon (2002). Prior to seafloor spreading, it is likely that the Woodlark Island was once continuous with Misima Island and would be a part of the same core complex. Woodlark Island is 33 km in width, while Misima

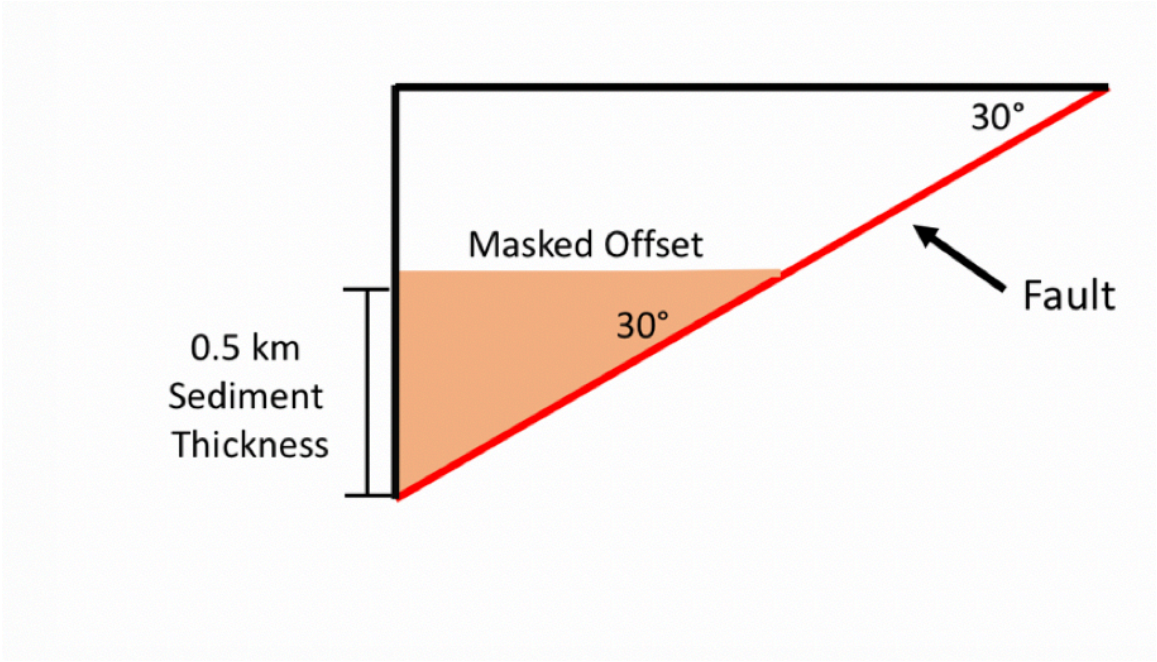

Figure 20. Simple illustration showing the effect of sediment cover on visible fault offsets. A 0.5 km, evenly distributed sediment package can mask up to 0.86 km of offset along a fault forming at 30°. Sediment is shaded orange, and the fault is shown with a red line.

Island is 8 km in width. Measuring extension based solely on their lateral extent would add an additional 41 km to the brittle faulting estimate. This does not take into account any detachment faulting that could have been involved in exhumation or any other unknown metamorphic core complexes. The metamorphic core complexes have likely been heavily faulted and there is a lack of geological studies in the islands. Foundered metamorphic core complexes could now be below sea level and could be hard to identify based on the quality of the seismic data. Additional extension could be also be validated based on the presence of a detachment fault, such as the one

depicted in the polyphase model (Figure 14) or those noted in Kington and Goodliffe (2008). To better constrain upper crustal characteristics, such as faulting and the composition of the upper crust including the presence of metamorphic core complexes, a long-offset seismic reflection and refraction study would need to be performed.

5.3: Potential Errors in Extension Estimates from Subsidence

The broad estimates used for the subsidence calculation using the Kington and Goodliffe (2008) method introduce an average error of +34 km, -41 km. To determine how subsidence is affected by changes in density and thicknesses of different layers, multiple numerical values were tested for these variables in Equation 2. These variables were not previously incorporated into the error estimates by Kington and Goodliffe (2008). As there is no constraint on sediment cover in the margins without seismic reflection data, sediment thicker than 0.5 km could be present in these regions. In addition, it is possible that a portion of the interpreted igneous basement could be pre-rift sediment. Pre-rift forearc basin sediments many kilometers thick were imaged in multi-channel seismic data west of Egum Atoll (Taylor and Huchon, 2002). These sediments likely underlie much of the northern margin of the Woodlark Basin and may be imaged as basement reflectors in low-fold seismic reflection data. Increasing sediment thickness in the basin to 1 km would increase extension estimates by ~69 km along line 180. Further, the continental crust density of 2800 kg m^{-3} is based on mafic crust at depth. If the Papuan Ultramafic Belt does not extend into the study area, the crust would be dominantly granitic, with a density of 2670 kg m^{-3}. This would reduce extension estimates by ~27 km at line 180.

Additionally, the assumption of Airy isostasy implies no flexural rigidity. Although hot and highly faulted continental crust will have low flexural rigidity, it will have some flexural strength. With flexural rigidity, the basin would be shallower than a basin formed purely by Airy

isostasy. For the current study, a broad estimate of the flexural properties in the basin is made. Assuming that the basin behaved rigidly, with the current basin depth only representing half of the depth that would be achieved in the case of zero flexural rigidity, extension along line 180 would be ~121 km.

The assumption that crustal cross-sectional area remained the same for the entire duration of continental rifting is also unlikely. Proximity to subduction zones and high heat flow could result in lower crustal flow. If this were the case, extension would be overestimated. Using a block model as an example (Figure 21), if the pre-rift thickness was 35 km and the initial basin width was 150 km, the total area along a 2-D profile would be 5250 km^2. If area was conserved and the crust thinned to 25 km, the width of the crust would be 210 km, and the total extension would be 60 km. If 20% of the crust had been incorporated into the mantle, the total pre-rift area

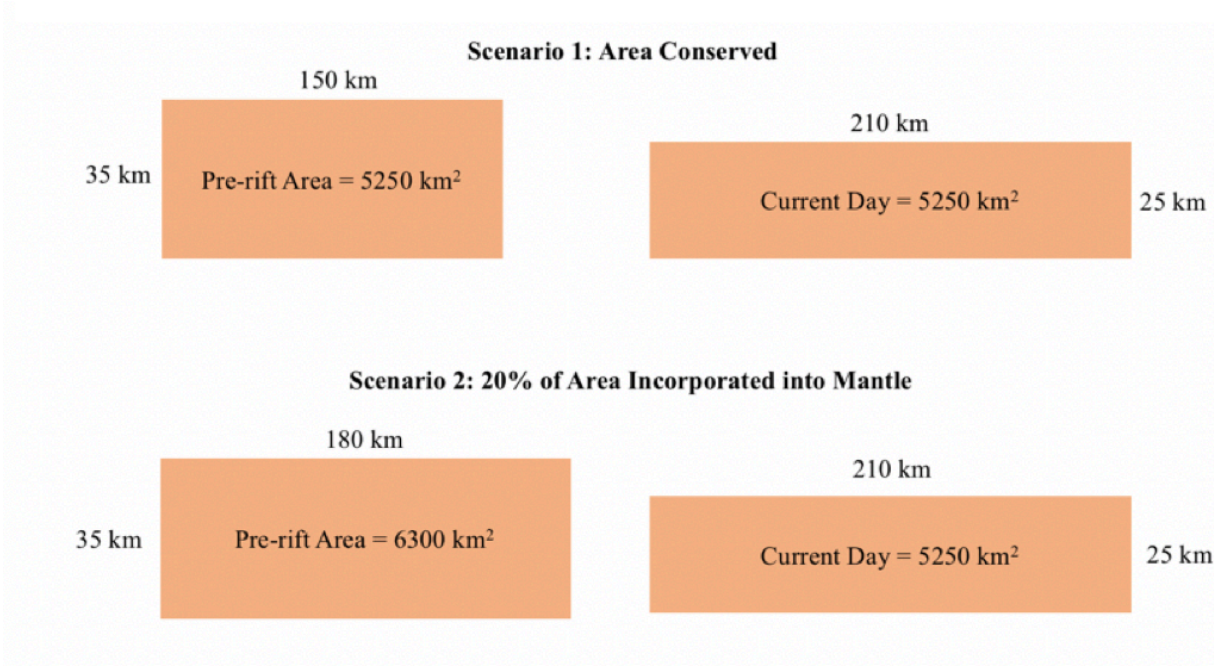

Figure 21. Simple block diagram illustrating the impact of maintaining crustal area in an extending basin. Blocks on the left indicate pre-rift crust. Blocks on the right indicate the crust of the present day basin. If crust is incorporated into the mantle, less extension will occur.

would have instead been 6300 km^2 at the initiation of rifting. Maintaining an initial crustal

thickness of 35 km, the initial basin width would be 180 km. In this case, half of the amount of extension (30 km) would have occurred. This calculation implies that if area is not conserved in the Woodlark basin, then the amount of extension estimated from subsidence could be half of that determined in Section 4.2.

From core data logged by Goodliffe et al. (2002) in the western Woodlark Basin, there is evidence that the basin was at sea level during rifting, between 5.23 and 5.39 Ma. However, assuming that the basin was at sea level with a crustal thickness of 35 km at the initiation of rifting is probably an underestimate. Taylor and Huchon (2002) looked at the rifting history in the basin using core and borehole data, and while some portions of the basin were likely at sea level during rifting, the rift zone probably formed in a zone of weakness associated with a significant mountain range and arc resulting from continental collision and subduction of the Australian plate under the Papuan Plateau. Based on the refraction study conducted on the Papuan Plateau, 2 km of paleoelevation corresponds to a 50 km thick crust (Finlayson et al., 1976). This would require far more extension to reach the current basin depth. Based on the simple block calculation, where the current basin is 210 km wide (at ~152°E) and the crustal thickness is 25 km, the total area along a 2-D profile would be 5250 km^2 with an initial basin width of 150 km. If pre-rift crustal thickness was 50 km and area was maintained during rifting, the initial basin width would only be 105 km. Therefore, extension in the basin would increase from 60 km (35 km pre-rift crustal thickness) to 105 km (50 km pre-rift crustal thickness). To better understand the pre-rift crustal thickness and to determine the current Moho depth in discrete areas of the basin, an active source ocean bottom seismometer study could be undertaken to characterize deeper structures.

5.4: Potential Errors in Extension Estimates from Euler Pole estimations

If the extension estimates predicted by the brittle faulting and subsidence methods are accurate, then this would imply that the Euler pole estimates do not accurately predict continental extension rates. The locations of the Euler poles are well constrained at the 95% confidence interval (Figure 2). One possible source of error is misidentification of fracture zone azimuths; however, the fault traces are easily identifiable due to thin sediment cover. The largest source of error would be associated with spreading rates prior to 3.33 to 3.58 Ma (chron 2A.3n) not being as well constrained due to the lack of a conjugate chron to the north of the spreading center in the far east of the basin. This portion of oceanic crust was subducted beneath the Solomon Islands. Using the results from Taylor et al. (1999) (Figure 15) to determine extension back to 3.58 Ma, the predicted width of stretched continent in the basin at line 180 was 118 km, for instance. This value is 49% of the predicted width at 6 Ma; therefore, this lack of constraint would impact 2.42 million years of extensional history. However, there is no indication that there was a drastic change in the rate of total plate motion or the Euler pole location prior to 3.58 Ma (Taylor et al. 1999) and, thus, the rates extrapolated back to 6 Ma are likely accurate.

5.5: The Possibility of a Third Plate

If the strike-slip Nubara Fault continues to the southwest along the Woodlark Rise, a third plate exists in the basin (Figure 1). The presence of this plate, bounded by the Nubara Fault to the south and the Trobriand Trough to the north, would reduce the northern margin width by ~56 km along the north-south profiles. Kington and Goodliffe (2008) ignored the possibility of this third plate in their calculations, but if it exists, the plate would encompass a majority of the northern portion (~111 km) of their study area and likely would have drastically changed their

estimates. Using the subsidence and brittle faulting estimates where the third plate affects the current study area, ~13 km of extension in the northeast and ~15 km of extension in the northwest is lost. In addition, this indicates that Woodlark Island would not be a potential conjugate metamorphic core complex to Misima Island, decreasing the associated error estimates for brittle faulting. Extension estimates from Euler pole kinematics are a function of current basin width. Pre-rift width and calculated stretched width are estimated from these values, excluding the oceanic crust. Therefore, a narrower basin would decrease the overall extension predicted from Euler pole kinematics. However, as the predicted extension rates do not change, extension estimates from Euler pole kinematics will still be larger than the extension estimates of brittle faulting. For the subsidence method, the third plate would decrease extension due to a smaller final width and area for the basin. Therefore, a third plate would further increase the discrepancy between Euler pole kinematics and subsidence and brittle faulting estimates.

5.6: Is the Kington and Goodliffe (2008) model necessary?

Based on the potential sources of error presented in Table 4, it is evident that the methods produce results that are not well-constrained. Large sources of error could come from misinterpretations of sediment cover thickness, unidentified core complexes, poorly constrained Euler poles during the early rifting history, and the assumption of zero flexural rigidity. Using line 180, a 0.5 km thickness of syn-rift sediment along the line could mask 58 km of extension. A metamorphic core complex could add ~100 km of extension, based on the sizes of Misima and Woodlark Islands and the detachment fault that formed them. Extension could be reduced by a three-plate solution (-13 km) or by a smaller amount of subseismic faulting (-9 km). Assuming that the basin behaved with some rigidity doubles the amount of extension (+61 km). The extension estimates from Euler pole kinematics could decrease by 49% if extension was only

extrapolated back to 3.58 Ma. These scenarios were tested for each seismic line (Table 4). Based on the estimate of maximum error for each line, it is possible that all three estimates of extension could agree. It is thus not necessary for this study to call upon the Kington and Goodliffe (2008) model to explain the results. The well-established models of pure and simple shear with constant extension rates over lithospheric depth may suffice.

Table 4. *Summary of extension estimates based on the methods from Kington and Goodliffe (2008) and additional potential sources of error for these methods.*

	Extension from Brittle Faulting (km)	Extension from Subsidence (km)	Extension from Euler Pole Kinematics (km)	Maximum Error Due to Brittle Faulting Assumptions (km)	Maximum Error Due to Subsidence Parameters (km)	Maximum Errors from Euler Pole Kinematics (km)
Line 100	68.5 (+ 47, -39)	68.15 (+33, -40)	202	+121, -18	+137, -49	-86
Line 140	78.8 (+48, -42)	76.67 (+30, -52)	223	+152, -20	+137, -42	-104
Line 150	92.1 (+56, -49)	71.75 (+33, -43)	224	+156, -20	+138, -50	-99
Line 160	90.4 (+59, -48)	64.14 (+37, - 38)	230.5	+159, -21	+132, -58	-110
Line 180	86.3 (+58, -45)	60.08 (+35, -34)	233	+158, -22	+130, -53	-115
Line 190	87.3 (+58, -45)	69.67 (+34, -40)	238	+163, -19	+125, -52	-119
Line 200	78.2 (+57, -43)	79.25 (+36, -47)	234	+170, -19	+151, -53	-113

CHAPTER 6: CONCLUSIONS

The main conclusions of this thesis are as follows:

- Kington and Goodliffe (2008) proposed that incorporating polyphase and subresolution faulting into brittle extension estimates greatly increases the amount of extension observed in a rift zone. Applying their methods to the current study supports this hypothesis. Therefore, it is possible that in other studies of rift basins where polyphase and subresolution faulting are not incorporated, brittle faulting is underestimated.
- The extension estimates based on subsidence from Kington and Goodliffe (2008) could have large errors as a result of assuming no flexural rigidity, no sediment cover, instantaneous rifting, constant crustal area throughout rifting, and that extension began at sea level.
- Based on the current study, the Kington and Goodliffe (2008) model may not be necessary to explain the results due to the uncertainties associated with the different extension estimate methods. Instead, the well-established models of pure shear and simple shear with constant extension rates over lithospheric depth may suffice based on the rifting geometries observed in the basin.
- Fully constraining potential sources of error in extension across the Woodlark Basin will require further study. For example, faulting and composition of the upper crust could be characterized through a long-offset seismic reflection and refraction study. Deeper structure could be characterized through an active source ocean bottom seismometer study.

REFERENCES

Abers, G.A., Mutter, C.Z., Fang, J. (1997). Earthquakes and normal faults in the Woodlark-D'Entrecasteaux rift system, Papua New Guinea. *Journal of Geophysical Research 102*, 15301–15317.

Abers, G.A., Ferris, A., Craig, M., Davies, H., Lerner-Lam, A., Mutter, C., Taylor, B. (2002). Mantle compensation of active metamorphic core complexes at Woodlark rift in Papua New Guinea. *Nature 418,* 856-862.

Baldwin, S.L., Lister, G.S., Hill, E.J., Foster, D.A., McDougall, I. (1993). Thermochronologic constraints on the tectonic evolution of active metamorphic core complexes, D'Entrecasteaux Islands, Papua New Guinea. *Tectonics 12*, 611–628.

Cande, S.C., Kent, D.V. (1995). Revised calibration of the geomagnetic polarity timescale for the Late Cretaceous and Cenozoic. *Journal of Geophysical Research. B, Solid Earth and Planets, 100* (4), 6093–6095.

Cochran, J. R. (1981). The Gulf of Aden: Structure and evolution of a young ocean basin and continental margin. *Journal of Geophysical Research, 86*, 263–287.

Davies, H.L., Smith, I.E. (1971). Geology of eastern Papua. *Geological Society of America Bulletin, 82,* 3299–3312.

Davies, H.L., Jaques, A.L. (1984). Emplacement of ophiolite in Papua New Guinea. In: Gass, I.G., Lippar, S.J., Shelton, A.W. (Eds.), *Ophiolites and Oceanic Lithosphere* (Vol 13, pp. 341–350). Spec. Publ.

Davis, M., Kusznir, N.J. (2004). Depth-dependent lithospheric stretching at rifted continental margins. In: Karner, G.D., Kohlstedt, D., Driscoll, N., Taylor, B. (Eds.), *Rheology and deformation of the lithosphere at continental margin* (pp. 92–137).

Driscoll, N.W., Karner, G.D. (1998). Lower crustal extension across the Northern Carnarvon basin, Australia: Evidence for an eastward dipping detachment. *Journal of Geophysical Research, 103,* 4975–4991.

Finlayson, D. M., Muirhead, K. J., Webb, J. P., Gibson, G., Furumoto, A. S., Cooke, R. S., Russel, A. J. (1976). Seismic investigation of the Papuan Ultramafic Belt. *Geophysical Journal International, 44* (1), 45-49.

Goodliffe, A.M., Taylor, B., Martinez, F., Hey, R., Maeda, K., Ohno, K. (1997). Synchronous reorientation of the Woodlark Basin Spreading Center. *Earth and Planetary Science Letters, 146* (1), 233–242.

Goodliffe, A.M., Taylor, B., Martinez, F. (1999). Data report: marine geophysical surveys of the Woodlark Basin region. In: Taylor, B., Huchon, P., Klaus, A., et al. (Eds.), Proc. ODP, Init. Repts. 180, 1–20 [CD-ROM]. Available from: Ocean Drilling Program, Texas A&M University, College Station, TX 77845-9547, U.S.A.

Goodliffe, A.M. (1998). *The rifting of continental and oceanic lithosphere: observations from the Woodlark Basin* (Ph.D. thesis). Univ. Hawaii, Honolulu.

Goodliffe, A.M., Martinez, F., Taylor, B., Lewis, T.J., Taylor, A.E., Screaton, E.J. (2000). *The Geothermal signature of continental breakup: results from the Woodlark Basin.* Poster.

Goodliffe, A.M., Taylor, B., Karner, G. (2002). Correlations between seismic logging, and core data from ODP leg 180 sites in the western Woodlark Basin. *Proceeding of the Ocean Drilling Program, Scientific Results, 180*, 1-25.

Goodliffe, A.M., Taylor, B., (2007). The boundary between continental rifting and seafloor spreading in the Woodlark Basin, Papua New Guinea. In: Karner, G.D., Manatschal, G., Pinhiero, L.M. (Eds*.), Imaging, Mapping and Modelling Continental Lithosphere Extension and Breakup, 282*. Geological Society, London, pp. 213–234. Special Publications.

Huismans, R., Beaumont, C., (2014). Rifted continental margins: The case for depth-dependent extension. *Earth and Planetary Science Letters, 407,* 148-162. doi 10.1016/j.epsl.2014.09.032

Kington J., Goodliffe, A.M. (2008). Plate Motion and continental extension at the rifting to spreading transition in Woodlark Basin, Papua New Guinea: Can oceanic plate kinematics be extended to continental rifts? *Tectonophysics, 458*, 82-95. doi 10.1016/j.tecto.2007.11.027

Kusznir, N.J., Hunsdale, R., Roberts, A.M. (2004). Timing of depth-dependent lithosphere stretching on the S Lofoten rifted margin offshore mid-Norway; pre-breakup or post-breakup? *Basin Research, 16* (2), 279-296.

Lavier, L.L., Manatschal, G. (2006). A mechanism to thin the continental lithosphere at magma-poor margins. *Nature 440*, 324–328.

Lister, G.S., Davis, G.A. (1989). The origin of metamorphic core complexes and detachment faults formed during Tertiary continental extension in the northern Colorado River region, U.S.A. *Journal of Structural Geology, 11* (1/2), 65-94.

Little, T. A., Baldwin, S.L., Fitzgerald, P.G., Monteleone, B, (2007). Continental rifting and metamorphic core complex formation ahead of the Woodlark spreading ridge, D'Entrecasteaux Islands, Papua New Guinea, *Tectonics, 26,* TC1002. doi:10.1029/2005TC001911

McKenzie, D.P. (1978). Some remarks on the development of sedimentary basins. *Earth Planet. Sci. Lett., 40*, 25–32.

McKenzie, D.P., Jackson, J., (2002). Conditions for flow in the continental crust. *Tectonics, 21, 5-1 – 57. doi:10.1029/2002TC001394*

Martinez, F. & Cochran, J. R. (1988). Structure and tectonics of the northern Red Sea: Catching a continental margin between rifting and drifting. *Tectonophysics, 150*, 1–32.

Martinez, F., and Taylor, B., Goodliffe, A., (1999). Contrasting styles of seafloor spreading in the Woodlark Basin: Indications of rift-induced secondary mantle convection. *Journal of Geophysical Research, 104*, 12,909-12,926.

Martinez, F., Taylor, B., Goodliffe, A. (2001). Metamorphic core complex formation by density inversion and lower crust extrusion. *Nature, 411*, 930–934.

Reston, T. J. (2005). Polyphase faulting during the development of the west Galicia rifted margin. *Earth and Planetary Science Letters, 237* (3–4), 561–576.

Reston, T.J., Leythaeuser, T., Booth-Rea, G., Sawyer, D., Klaeschen, D., Long, C. (2007). Movement along a low-angle normal fault: The S reflector west of Spain. *Geochemistry, Geophysics, Geosystems, 8.* 1-14. doi:10.1029/2006GC001437

Taylor, B., Goodliffe, A., Martinez, F., Hey, R. (1995). Continental rifting and initial seafloor spreading in the Woodlark Basin, *Nature*, *374*, 534-537.

Taylor, B., Goodliffe, A.M., Martinez, F. (1999). How continents break up—insights from Papua New Guinea. *Journal of Geophysical Research, 104* (B4), 7497–7512.

Taylor, B., Huchon, P. (2002). Active continental extension in the western Woodlark Basin: a synthesis of Leg 180 results. In: Taylor, B., Huchon, P., Klaus, A. (Eds.), *Proc. ODP, Sci. Results, 180*, 1–36.

Turcotte, D.L., Schubert, G. (2002). *Geodynamics.* Cambridge University Press.

Walsh, J., Watterson, J., Yielding, G. (1991). The importance of small-scale faulting in regional extension. *Nature, 351*, 391–393.

Wernicke, B. (1985) Uniform-sense normal simple shear of the continental lithosphere, *Can. J. Earth Sci., 22*, 108-12.

APPENDIX A

Figures A1-A6 show the uninterpreted seismic reflection profiles along lines 100, 140-160, and 190-200 as well as a larger-scale view of a representative segment of each line and an interpretation of the representative segment showing visible faults and horizons. A description of major structural features for each seismic line is also included.

Line 100:

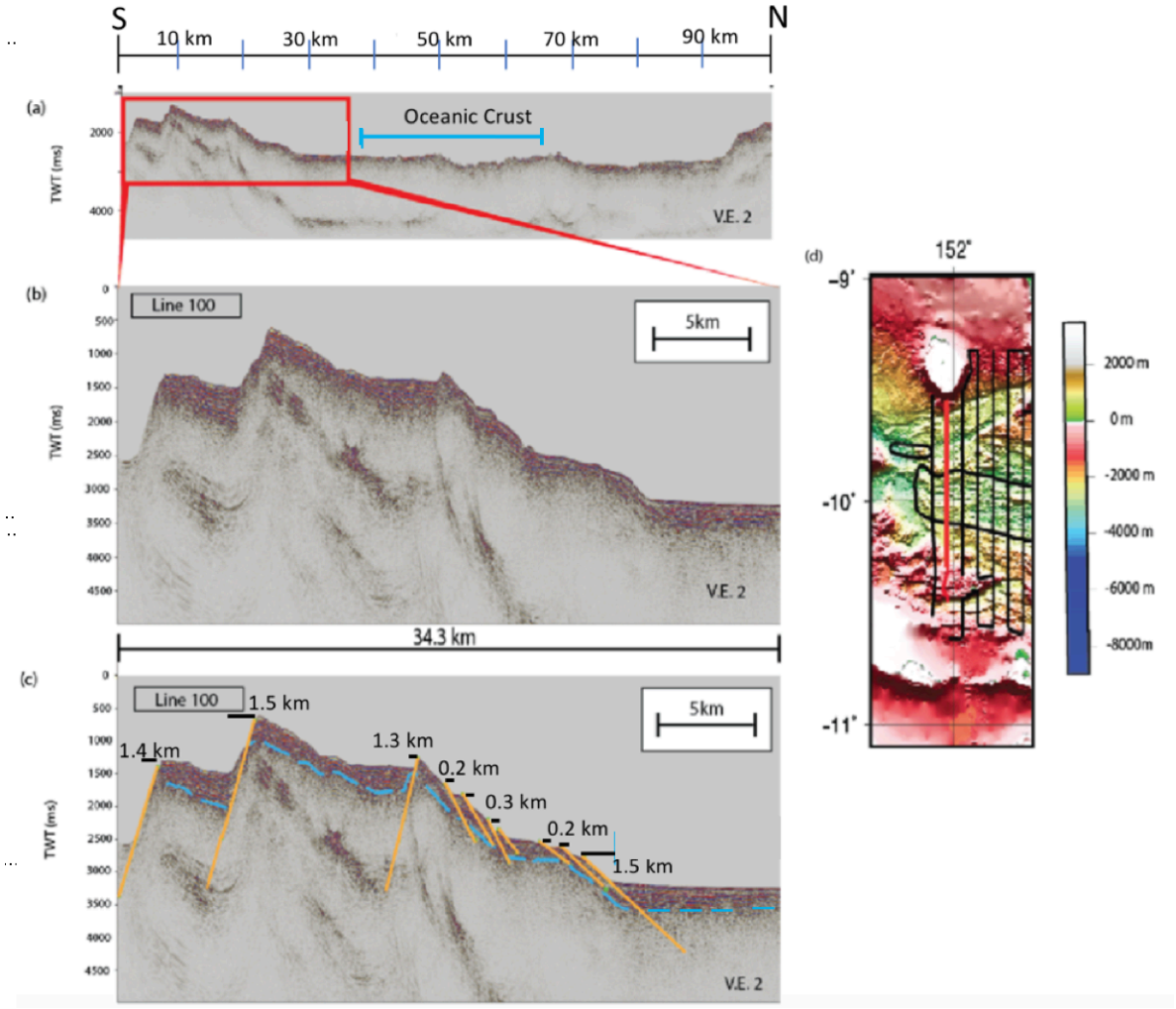

Figure A1. (a) Seismic Line MW9304-100. Vertical exaggeration is 2. The red box indicates the location of the detailed section shown in panels (b) and (c). The extent of oceanic crust (OC) is shown by the solid blue line. The map in (d) shows the location of the seismic reflection line (highlighted in red). (b) Uninterpreted and (c) interpreted seismic reflection data. Faults are shown by the orange lines. The basement reflector is shown by a dashed blue line.

Starting at the southernmost portion of the seismic line, three continental blocks, separated by normal faults dipping at ~40°S and spanning 26 km, are evident (Figure A1). Heaves range from 1.5 to 1.3 km. A sediment package with ~0.4 km thickness infills the down-thrown portions of the fault blocks. A minimum water depth of ~0.8 km is reached on the

second-most southern continent block (at 10 km, Figure A1). The northernmost of these continental blocks is more heavily faulted on the northern side, approaching the continent-ocean boundary. These faults are more closely spaced, occurring every 1 to 1.5 km and dipping between ~25°N and ~35°N. Heaves here range from 0.2 to 0.3 km. Thinner sediment cover (~0.1 km thick) is evident along these faults. These northward dipping faults down-step from a water depth of ~0.7 to ~1.7 km at the continent-ocean boundary (at 38 km, Figure A1) over 28 km. Ocean lithosphere (maximum water depth of ~2.2 km) outcrops on the seafloor for 38 km (spreading segment 1, Figure 3). On the other side of the continent-ocean boundary (at 65 km, Figure A1), the seismic reflection line covers 35 km of the northern margin. Water depth gradually decreases to ~1.7 km over a distance of 30 km to the north. Sediment thickness is ~0.5 km. Visible heaves (0.2 to 0.4 km) are evident in the northernmost portion of the seismic line. These heaves are interpreted as five closely spaced (0.5 km) faults that primarily dip at ~35°S to ~40°S, while up-stepping to the north. The northernmost fault block (at 95 km, Figure A1) is covered with ~0.6 km of sediment.

A total of twenty-five faults were interpreted for line 100. Observable fault heaves were summed to produce 11.6 km of extension. Based on a data pixel size of 200 m, an error bar of ±10 was given to this estimate. Extension from subresolution faulting added 5.8 km of extension. Polyphase faulting increased the estimate by ~25 km. Extension where there is no seismic coverage increased extension by 26 km (+22, -14). Total extension from brittle faulting was 68.5 km (β of 1.37; +0.29, -0.16). The maximum error associated with this line is +121 km, -16 km.

Line 140:

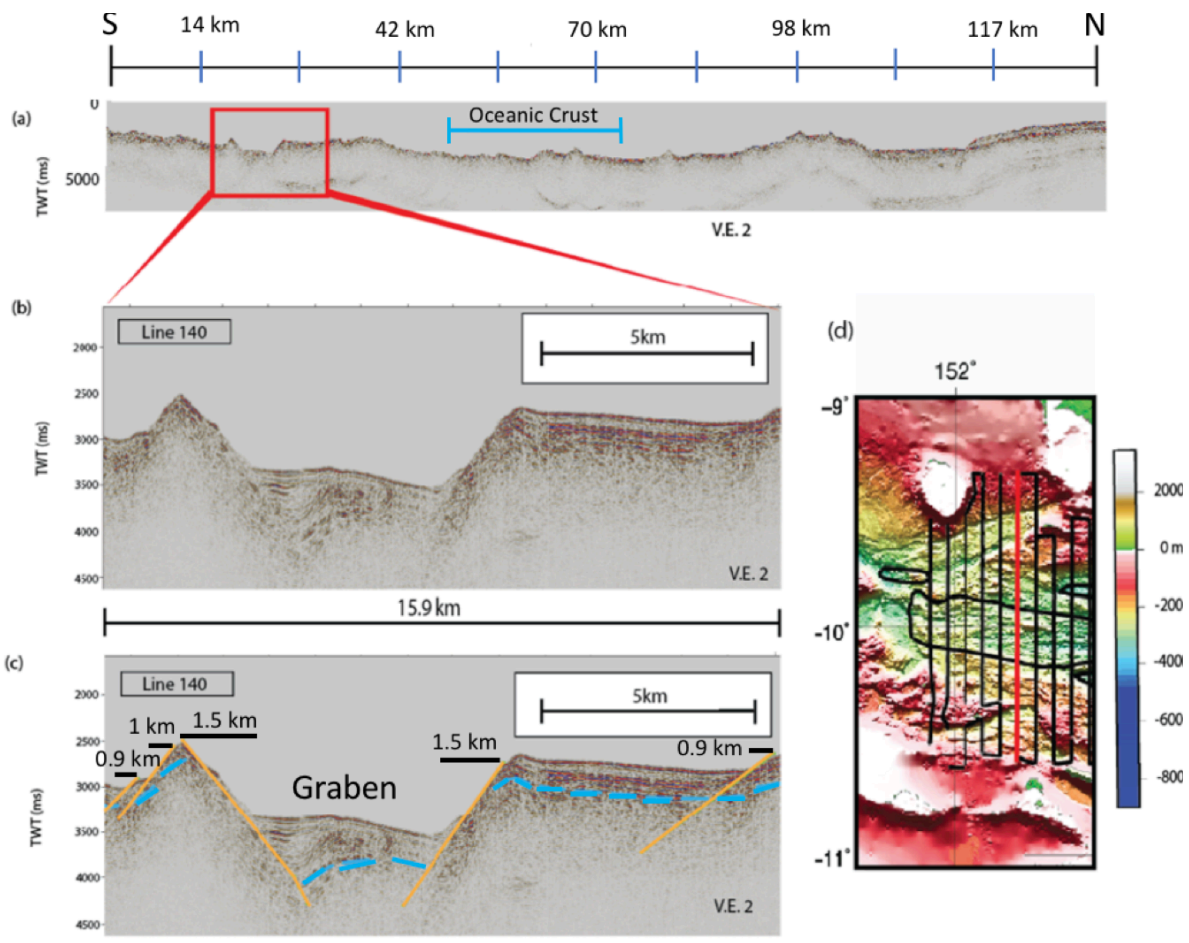

Figure A2. As Figure A1 but for seismic line MW9304-140.

Starting at the southernmost portion of the seismic line, there are a series of normal faults with heaves ranging from 0.1 to 0.6 km. There is a sediment infill of ~0.2 km. The faults dip at ~40°N and down-step from water depths of ~1.3 to ~2.2 km over 16 km. A horst (0.5 km wide, ~1.9 km in water depth) and graben (5 km wide, ~2.5 km in water depth) is evident to the north of these faults (Figure A2). The normal faults bounding these features have heaves of 0.9 to 1.5 km and dip at ~45°N and ~45°S, respectively. The graben contains a ~0.5 km thick sediment package. Another horst (~2 km water depth) to the north is 8 km wide (at 25 km, Figure A2). A series of down-stepping faults (heaves 0.1 to 0.4 km) begin with the fault bounding the northern

side of the horst. Water depths increase from ~1.2 to ~2.8 km at the continent-ocean boundary (at 49 km, Figure A2). Oceanic lithosphere (spreading segment 1, Figure 3) is present for 25 km. At the northern continent-ocean boundary (74 km, Figure A2), a continental fault block extends for 28 km. Faults (heaves 0.8 to 0.2 km, dipping at ~45°N) on this block up-step from ~2.52 to ~2.6 over 8.4 km. To the north, faults (heaves 0.5 to 1.4 km, dipping at ~30°S) on the continental block down-step from ~2.4 km to ~2.6 km over 9 km. The northernmost fault (at 109 km, Figure A2) forms the southern side of a graben structure (sediment infill of ~0.7 km) that extends 13.5 km to the north. A series of up-stepping faults are located to the north of the graben, beginning with a fault (heave of 0.3 km) dipping at ~50°S (at 114 km, Figure A2). Water depths decrease from ~2.4 to ~1.4 km over the next 19 km. The sediment package over this portion of the line is ~1.0 km thick and masks the heaves of the remaining faults.

A total of sixty-one faults were recognized along line 140. Observable fault heaves were summed to produce 24.5 km of extension. Based on a data pixel size of 200 m, an error bar of ±17 was given to this estimate. Extension from subresolution faulting added 12.25 km of extension. Polyphase faulting increased the estimate by ~28 km. Extension where there is no seismic coverage increased extension by 14 km (+14, -8). Total extension from brittle faulting was 78.8 km (β of 1.53; +0.49, -0.22). The maximum error associated with this line is +152 km, -18 km.

Line 150:

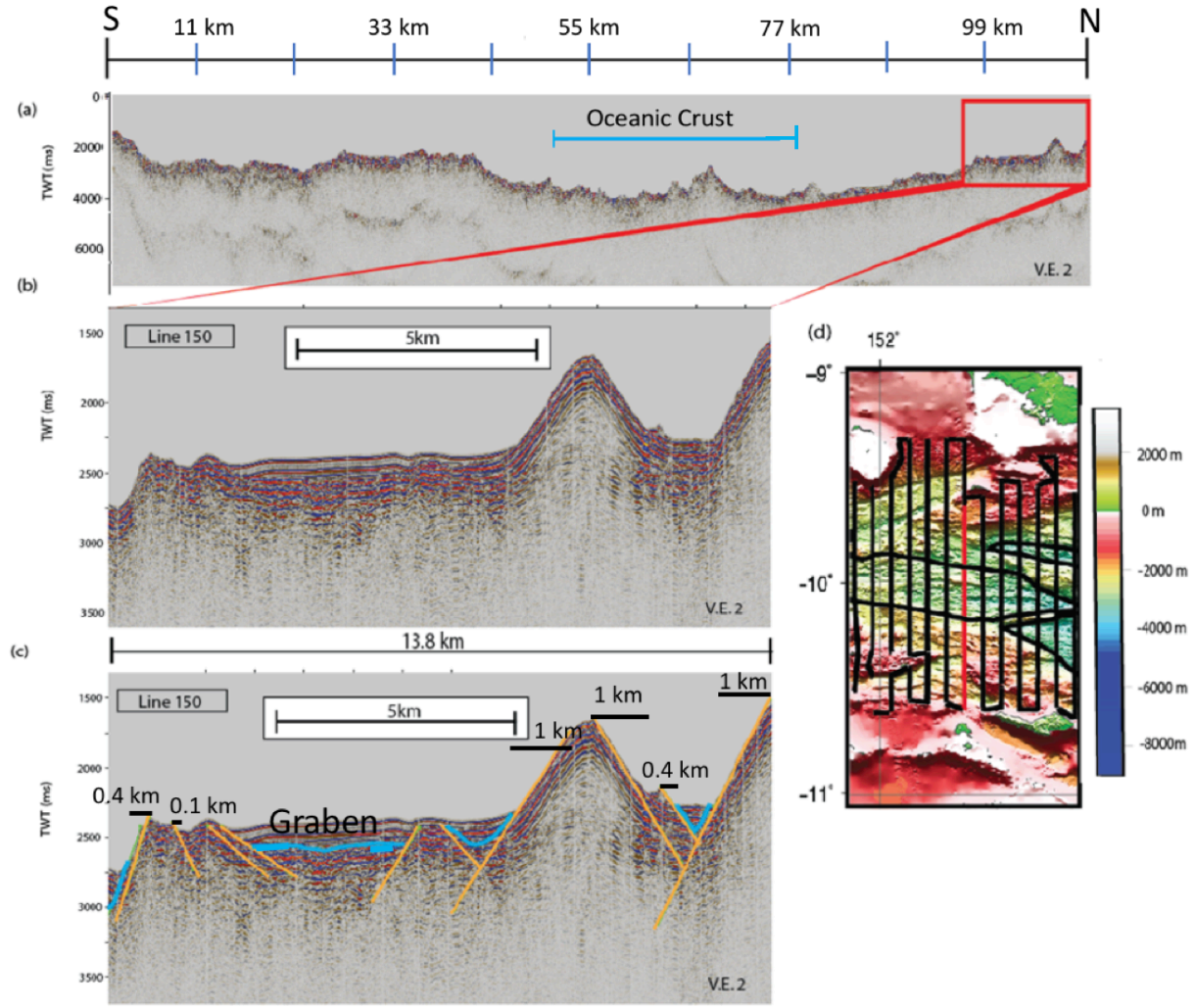

Figure A3. As Figure A1 but for seismic line MW9304-150.

Beginning at the southernmost portion of the seismic line, normal faults (dipping ~30°N, heaves 0.2 to 1 km) down-step from water depths of ~1.1 to ~2.1 km over 14 km. A graben (2.4 km across, ~2.1 km in water depth) and horst (5.7 km across, ~1.8 km in water depth) follow these normal faults. The faults that form the horst dip at ~40°S on the southern side of the horst and ~35°N to the north of the horst. At 23 km (Figure A3), faults up-step from a water depth of ~1.8 to ~1.5 km over 4.4 km. To the north of these faults, no surface offsets are observed for 8 km due to a sediment package that is ~0.4 km thick. Directly north of this sediment package (at

32 km, Figure A3), faults dipping at ~40°N (heaves of 0.3 to 0.7 km) down-step from ~1.5 to ~2.9 km water depth approaching the continent-ocean boundary (at 50 km, Figure A3). Oceanic lithosphere outcrops for 25 km. The maximum water depth is reached is ~3 km. To the north of the continent-ocean boundary, a series of faults (dipping at ~35°S, heaves of 0.1–0.4 km) up-step from water depths of ~2.7 to ~1.9 km over 16 km. Another sediment package (~0.5 km thick) extends for 7 km to the north of these faults, masking any further offsets (Figure A3). A horst structure (0.8 km across, ~1.2 km in water depth) is evident to the north of this sediment package, bounded by ~45° faults on either side (heaves of 1 km). A graben (1.6 km across, ~1.7 km in water depth) separates this horst from another horst formed by a fault dipping ~45°S. This extends to the end of the seismic line for 1.3 km.

A total of sixty-five faults were recognized along line 150. Observable fault heaves were summed to produce 26.8 km of extension. Based on a data pixel size of 200 m, an error bar of ±19 was given to this estimate. Extension from subresolution faulting added 13.4 km of extension. Polyphase faulting increased the estimate by ~28 km. Extension where there is no seismic coverage increased extension by 24 km (+20, -13). Total extension from brittle faulting was 92.1 km (β of 1.57; +0.51, -0.26). The maximum error associated with this line is +156 km, -18 km.

Line 160:

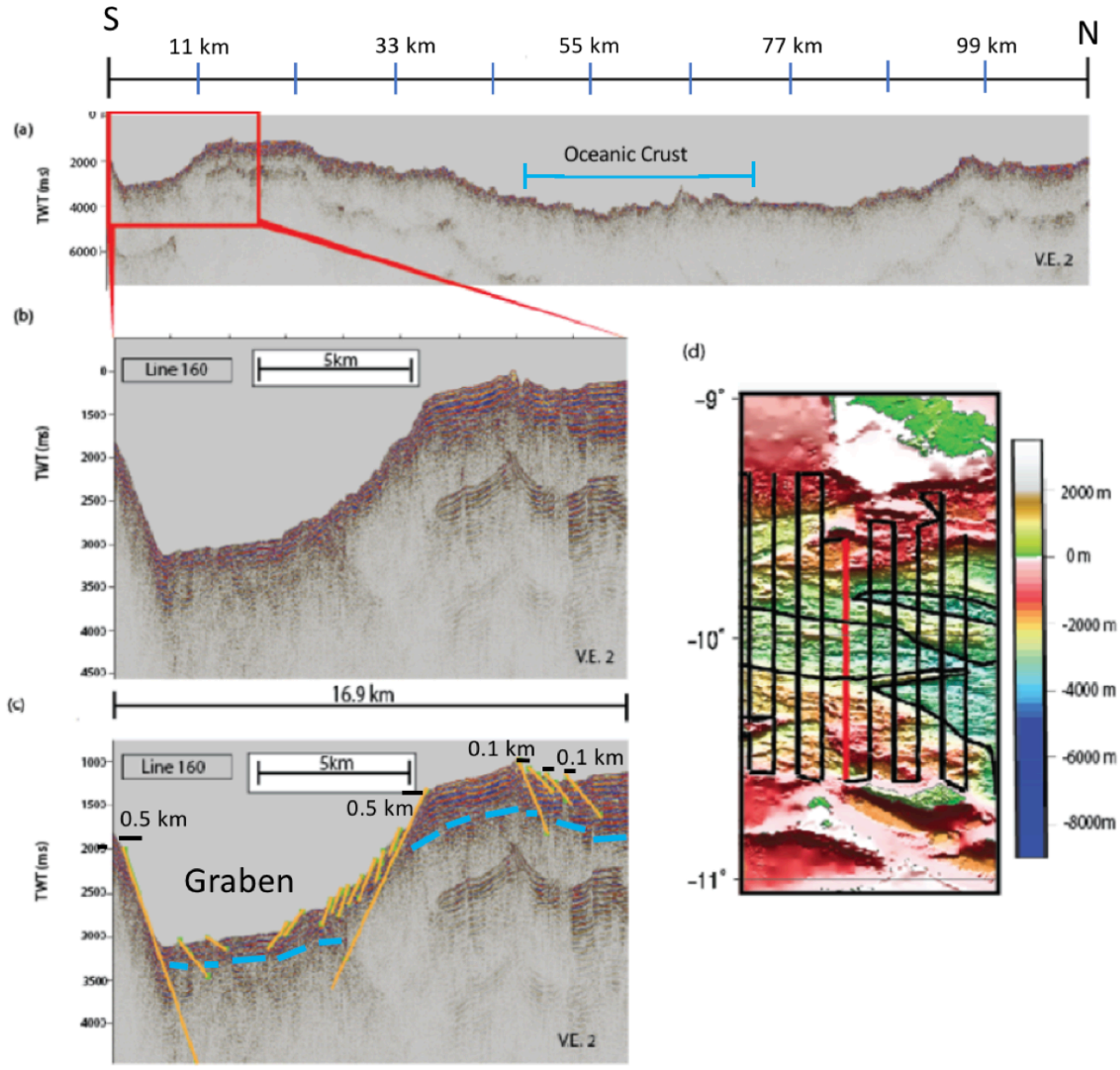

Figure A4. As Figure A1 but for seismic line MW9304-160.

Beginning at the southernmost portion of the seismic line, a fault that extends off of the profile dips at ~50°N, forming a graben (9.5 km across, ~2.4 km in water depth) to the north (Figure A4). The graben contains several faults (heaves of 0.1 to 0.2 km, dipping at ~50°S), primarily up-stepping to the north from water depths of ~2.6 to ~0.9 km over 5 km. A horst (12 km across, ~0.8 km in water depth) begins to the north of the final up-stepping fault (at 10 km,

Figure A4). Faults (dipping at ~35°N to ~50°N, heaves of 0.1 to 0.5 km) down-step on the north side of the horst, from a water depth ~0.9 to ~3.1 km over 29.8 km, approaching the continent-ocean boundary at 47 km (Figure A4). Oceanic lithosphere outcrops for 23 km; the maximum water depth is ~3.8 km. The northern margin (at 69 km, Figure A4) begins with faults (dipping at ~35°S to ~45°S, heaves of 0.1 to 0.6 km) up-stepping from a water depth of ~2.9 to ~1.4 km over 15 km to the north. A graben (3 km across, ~2.2 km in water depth) is found to the north of these faults. A fault dipping at ~30°N with a heave of 0.7 km forms the southern side. Another fault dipping at ~40°S with a heave of 0.7 km forms the northern side. To the north of this fault (at 94 km, Figure A4), a horst (2 km across, ~1.4 km in water depth) and graben (6.7 km across, ~1.7 km in water depth) are separated by a fault that dips ~30°N with a heave of 0.5 km. The graben extends to the end of the seismic line and is infilled by ~0.9 km of sediment.

A total of sixty-nine faults were recognized along line 160. Observable fault heaves were summed to produce 28.3 km of extension. Based on a data pixel size of 200 m, an error bar of ±22 was given to this estimate. Extension from subresolution faulting added 14.15 km of extension. Polyphase faulting increased the estimate by ~28 km. Extension where there is no seismic coverage increased extension by 20 km (+20, -9). Total extension from brittle faulting was 90.4 km (β of 1.56; +0.53, -0.25). The maximum error associated with this line is +159 km, -19 km.

Line 190:

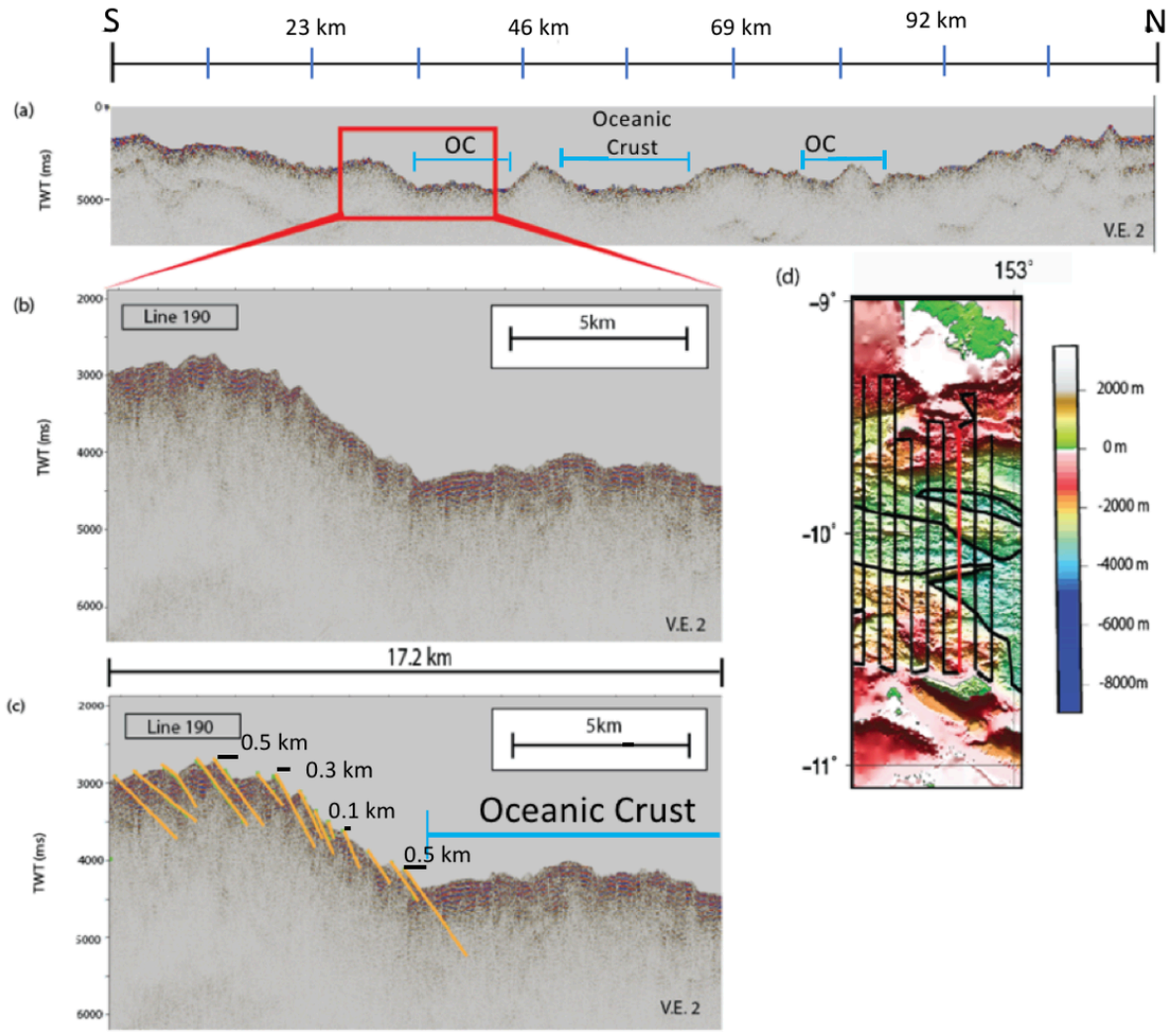

Figure A5. As Figure A1 but for seismic line MW9304-190.

Starting at the southernmost portion of the seismic line, a series of faults (heaves from 0.1 to 0.6 km, dipping at ~30°N) down-step from water depths of ~1.2 to ~1.7 km. The northernmost fault in this series (at 6 km, Figure A5) forms the southern side of a graben (3 km across, sediment infill 0.4 km thick). The northern side of the graben is separated from a horst (6.8 km across, water depth of 1.4 km, topped with sediment ~0.3 km thick) by a fault dipping at ~45°N (heave of 0.4 km). Further north (at 16 km, Figure A5), the sediment thins out to less

than ~0.1 km; faults (dipping at ~40°N) down-step from water depths of ~1.4 to ~2.5 km over 10 km. Heaves range from 0.3 to 0.5 km. To the north of these faults, sediment is again negligible. Water depths decrease from 3.3 to 2.7 km over 5 km. A horst structure is evident here, up-thrown by a fault (heave of 0.4 km) dipping at ~40°S. The northern side of the horst structure is formed from a fault with a heave of 0.2 km dipping at ~35°N. A series of faults (dipping at ~45°N with heaves from 0.2 to 0.5 km) down-step from ~2.1 to ~3.3 km over the next 6 km (Figure A5). The last of these faults marks the continent-ocean boundary at 35 km (Figure A5). Oceanic lithosphere outcrops for 11 km. Further to the north (at 46 km, Figure A5), there is an isolated continental block that is 8.7 km wide. Sediment coverage is negligible on this block. Water depths decrease from ~3.6 to ~2.3 km over 2.7 km along a series of normal faults (dipping at ~40°S to ~50°S, heaves from 0.2 to 0.4 km). Water depth increases from ~2.3 to ~3.4 km over the next 6 km, approaching the continent-ocean boundary at 50 km (Figure A5) on the northern side of the continental block. Faults on the northern side dip at ~35°N to ~50°N and have heaves of 0.2 to 0.4 km. Oceanic lithosphere outcrops to the north of these faults over the next 11 km. A second isolated continental block (13 km wide, topped by a sediment package ~0.2 km thick) is evident to the north of this oceanic lithosphere at 65 km (Figure A5). Water depths decrease from ~3.3 to ~2.3 km over 6 km along faults dipping ~30°S to ~45°S. Water depth then increases, approaching a graben (water depth of ~2.7 km, sediment infill ~0.3 km thick), followed by a horst (water depth of ~2.5 km, negligible sediment) on the northern portion of the continental blocks. Faults along these structures dip at ~40°N and ~50°S with heaves ranging from 0.1 to 0.5 km. Oceanic lithosphere (max water depth of ~3 km) outcrops to the north of the fault block at 76 km (Figure A5) for 8 km. The northern margin begins at 85 km (Figure A5). A series of horst and grabens gradually decrease in water depth (from ~3 to ~1.1

km) for the entire northern portion (35 km) of the seismic line. Grabens range from 13 to 32 km in width; typical sediment infill in these grabens is ~0.3 km thick. The northernmost graben (13 km wide) contains ~0.6 km of sediment infill. The northernmost horst (0.8 km wide) is the highest elevation block in the seismic section at ~0.8 km in water depth.

A total of seventy-three faults were recognized along line 190. Observable fault heaves were summed to produce 30.9 km of extension. Based on a data pixel size of 200 m, an error bar of ±21 was given to this estimate. Extension from subresolution faulting added 15.45 km of extension. Polyphase faulting increased the estimate by ~26 km. Extension where there is no seismic coverage increased extension by 13 km (+20, -7). Total extension from brittle faulting was 84.3 km (β of 1.51; +0.48, -0.21). The maximum error associated with this line is +163 km, -21 km.

Line 200:

At the southernmost portion of the seismic line, a fault dipping to the north with a heave of 1.4 km cuts through a fault block. The down-thrown portion (~2.1 km water depth, 7 km

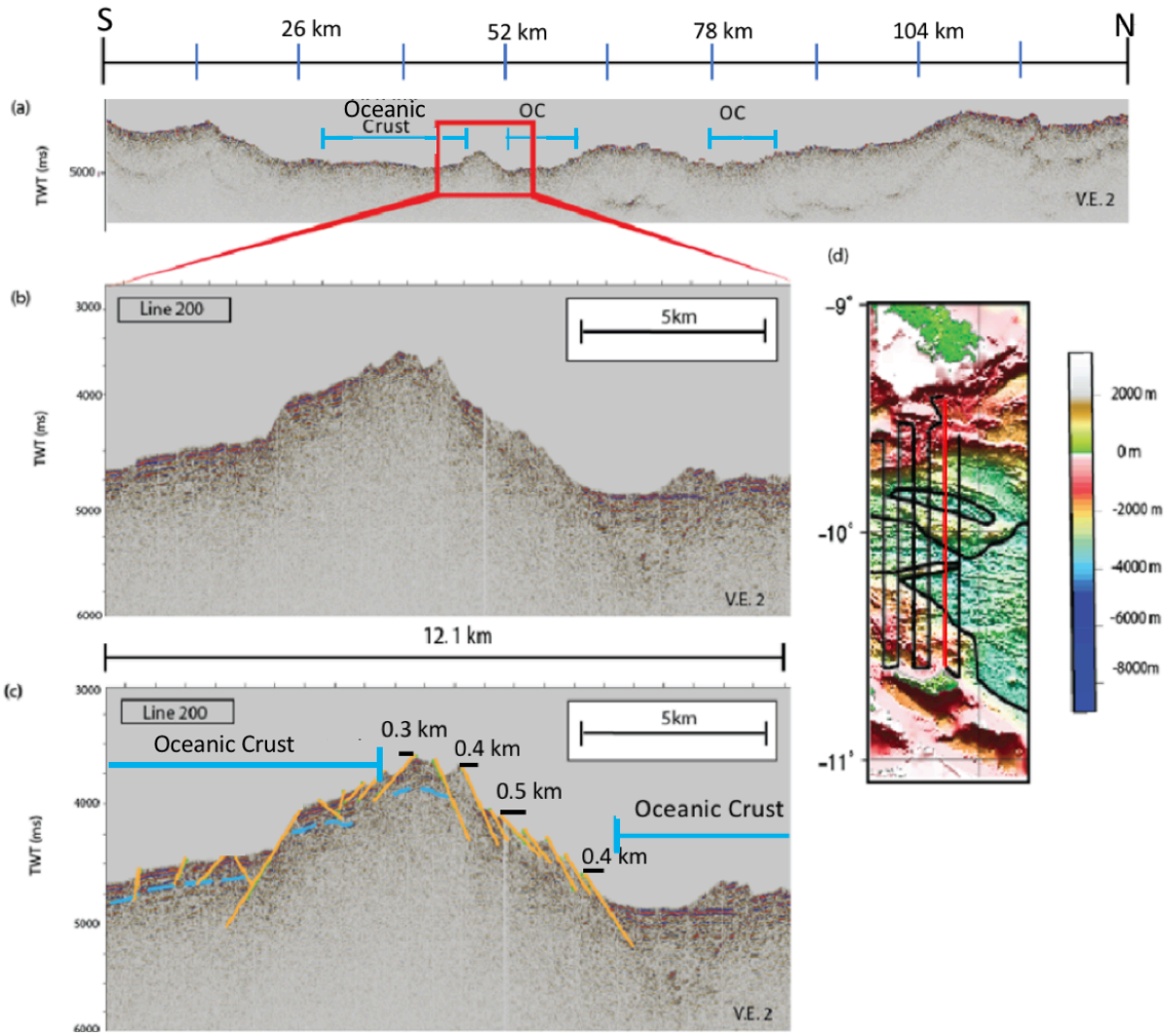

Figure A6. As Figure A1 but for seismic line MW9304-200.

wide) contains ~0.3 km of sediment and masks fault offsets at the surface from at distances of 0 to 13 km along the seismic line (Figure A6). Faults on the southern side of this block primarily dip at ~40°S and have heaves of 0.2 to 0.3 km. Water depths decrease on the southern side from ~1.8 to ~1.4 km over 5 km. On the northern side of the fault block (at 18 km, Figure A6), water depths increase from ~1.4 to ~3.4 km over a series of down-stepping faults (heaves from 0.1 to

0.7 km, dipping ~35°N to ~50°N) approaching the continent-ocean boundary at 30 km (Figure A6). Oceanic lithosphere outcrops for 17.8 km approaching an isolated continental block (4.8 km wide, topped with ~0.2 km of sediment). On the southern side of the continental block, water depth decreases from ~3.3 to ~2.7 km over a series of faults (dipping at ~45°S, heaves of 0.1 to 0.4 km). On the northern side of the continental block, water depths increase from ~2.7 to ~3.7 km over a series of faults (dipping at ~45°N, heaves of 0.2 to 0.3 km; Figure A6). To the north of this continental block, oceanic lithosphere outcrops for 8 km. Another isolated continental block is evident to the north of the oceanic lithosphere at 59 km (Figure A6). Along the southern side of this block, water depths decrease from ~3.4 to ~2.5 km over 9.9 km due to a series of up-stepping faults dipping at 45°S (heaves of 0.1 to 0.5 km). On the northern portion of the continental block, a series of horsts (0.6 to 1.2 km wide) and grabens (0.6 to 1.5 km wide, sediment infill of ~0.1 km) are present. Water depths generally increase from ~2.5 to ~3.3 across these structures. To the north of these grabens, oceanic lithosphere outcrops for 8 km (at 77 km, Figure A6). To the north of the oceanic lithosphere, the northern margin decreases in water depth from ~3.3 to ~1.1 km over 23 km due to up-stepping normal faults (dipping between ~35°S and ~45°S; heaves of 0.3 to 0.6 km). The northernmost 21 km of the seismic line is composed of a series of horsts (0.5 to 0.7 km wide, negligible sediment) and grabens (0.6 to 0.8 km wide, sediment packages ~0.7 km thick) formed by faults primarily dipping at ~40°N and ~50°S with heaves ranging from 0.2 to 1 km.

A total of eighty-one faults were recognized along line 200. Observable fault heaves were summed to produce 28.2 km of extension. Based on a data pixel size of 200 m, an error bar of ±23 was given to this estimate. Extension from subresolution faulting added 14.1 km of extension. Polyphase faulting increased the estimate by ~26 km. Extension where there is no

seismic coverage increased extension by 10 km (+19, -5). Total extension from brittle faulting was 76.2 km (β of 1.41; +0.40, -0.16). The maximum error associated with this line is +170 km, -21 km.

APPENDIX B

Figures B1-B7 show the bathymetry and crustal thickness along each seismic profile, plotted as a function of latitude between 8.5°S and 11.5°S. A description of the crustal thicknesses in relation to geologic features in the basin for lines 100, 140, 150-160, and 190-200 follows.

Line 100:

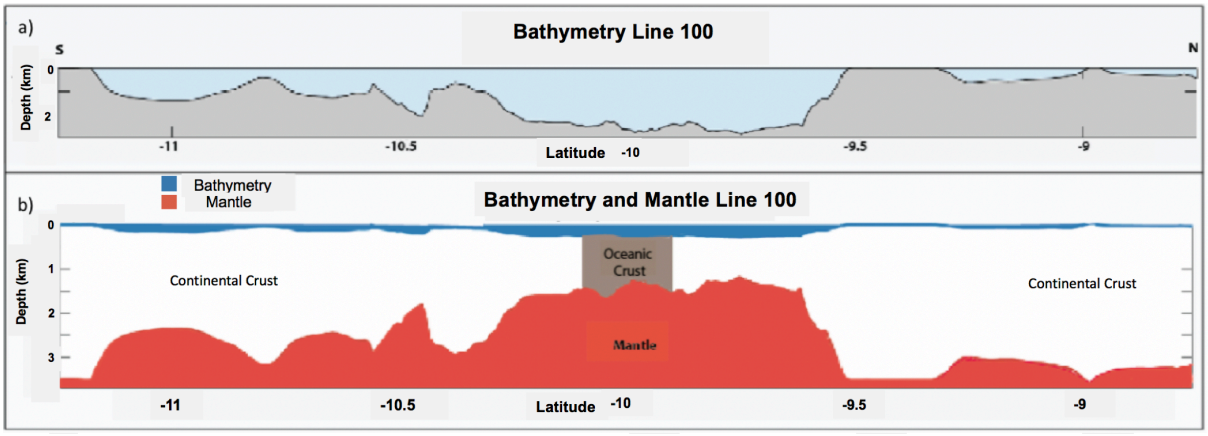

Figure B1. Crustal profile along seismic reflection line 100. (a) Bathymetry plotted as a function of latitude. (b) Bathymetry (blue) and calculated Moho depth (red) plotted as a function of latitude. Continental crust is shaded white. Oceanic crust is shaded dark grey.

The southernmost portion of line 100 (Figure B1) has thick crust (~33 km) over the Pocklington Rise. It thins to ~25 km in a basin to the south of the rise. A second ridge is located at 10.8°S, with a crustal thickness of ~32 km. A series of smaller rifted blocks are present approaching the continent-ocean boundary, with crustal thicknesses ranging from 20 to 30 km. Oceanic crust outcrops between 10.1°S and 9.9°S. The thickness of the oceanic crust is ~15 km. To the north of the continent-ocean boundary, the continental crust thickens to ~34 km at the Egum Atoll. To the north of the atoll, crustal thickness varies from ~30 to ~34 km towards the end of the line.

Line 140:

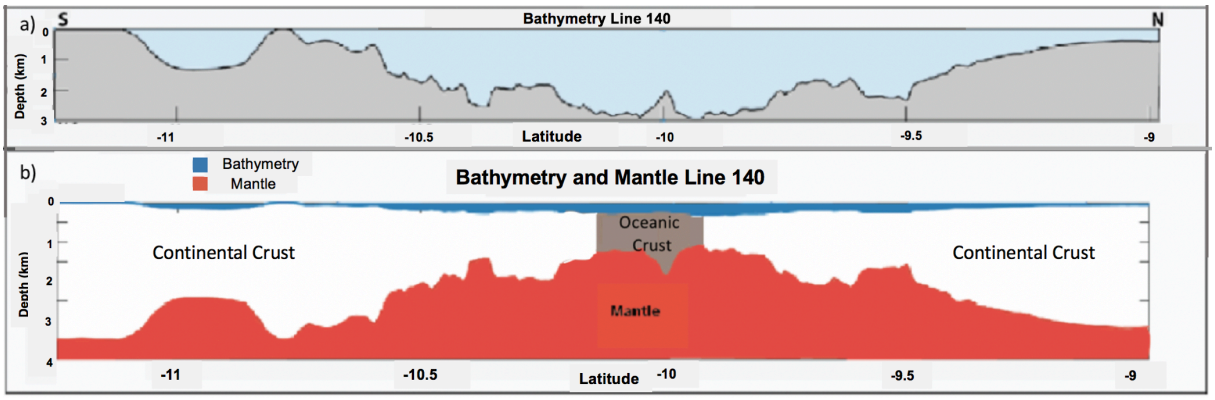

Figure B2. As Figure B1 but for seismic reflection line 140.

The southernmost portion of line 140 (Figure B2) has thick crust (~35 km) over the Pocklington Rise. The crust thins to ~25 km in a basin to the south of the rise. A second ridge is located at 10.8°S, with a crustal thickness of ~35 km. A series of smaller rifted blocks are present approaching the continent-ocean boundary, with crustal thicknesses ranging from ~15 to ~34 km. Oceanic crust outcrops between 10.25°S and 9.9°S. The thickness of the oceanic crust is ~14 km. To the north of the continent-ocean boundary, the continental crust thickens to ~24 km over a ridge. To the north of the ridge, crustal thickness increases from ~25 to ~32 km towards the end of the line.

Line 150:

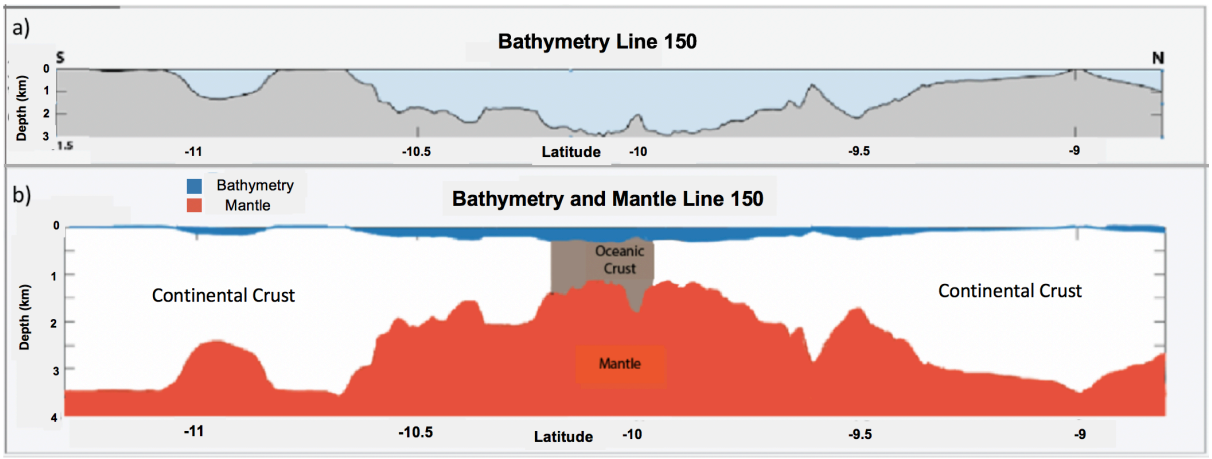

Figure B3. As Figure B1 but for seismic reflection line 150.

The southernmost portion of line 150 (Figure B3) has thick crust (~35 km) over the Pocklington Rise. The crust thins to ~25 km in a basin to the south of the rise. A second ridge is located at 10.75°S, with a crustal thickness of ~35 km. A series of smaller rifted blocks are present approaching the continent-ocean boundary, with crustal thicknesses ranging from ~15 to ~30 km. Oceanic crust outcrops between 10.18°S and 9.98°S. The thickness of the oceanic crust is ~14 km. To the north of the continent-ocean boundary, the continental crust thickens to ~30 km over a ridge. To the north of the ridge, crustal thickness decreases from ~30 to ~17 km due to a large basin. Further north, the crust thickens to ~35 km over the Woodlark Rise and then decreases gradually to ~30 km toward the north.

Line 160:

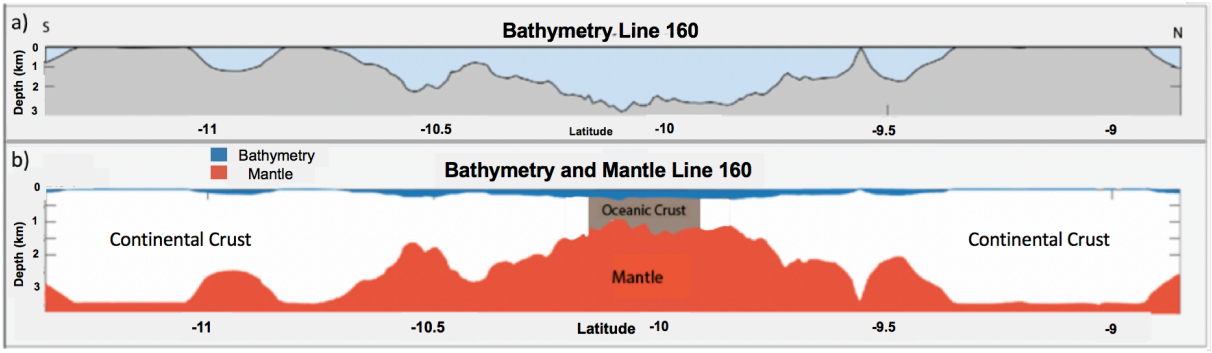

Figure B4. As Figure B1 but for seismic reflection line 160.

The southernmost portion of line 160 (Figure B4) has thick crust (~32 km) over the Pocklington Rise. The crust thins to ~25 km in a basin to the south of the rise. A second ridge is located at 10.75°S, with a crustal thickness of ~35 km. The crust then thins to ~17 km in a basin to the north of the ridge. A series of smaller rifted blocks are present approaching the continent-ocean boundary, with crustal thicknesses ranging from ~19 to ~29 km. Oceanic crust outcrops between 10.15°S and 9.85°S. The thickness of the oceanic crust is ~12 km. To the north of the continent-ocean boundary, continental crust thickens to ~34 km over a series of normal faults up-stepping to the north. Further north of the faults, crustal thickness decreases from ~34 to ~25 km due to a large basin. Past the basin, the crust thickens to ~34 km over the Woodlark Rise and Woodlark Island. It decreases gradually to ~31 km to the north of the rise due to the gradual slope.

Line 190:

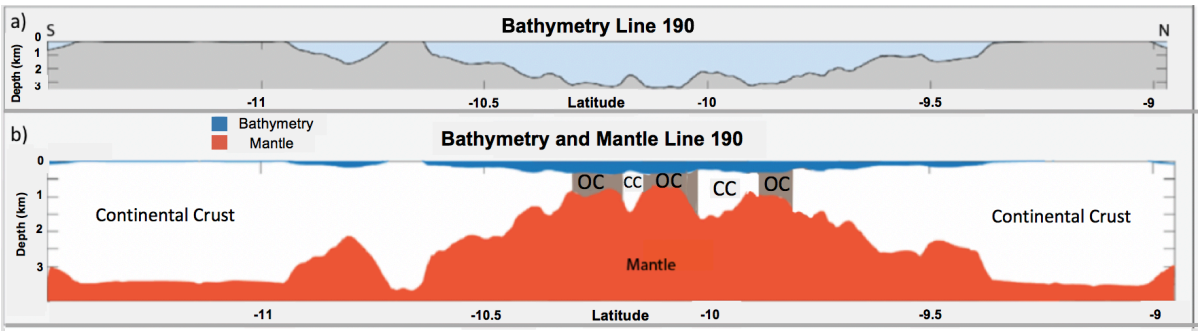

Figure B5. As Figure B1 but for seismic reflection line 190.

The southernmost portion of line 190 (Figure B5) has thick crust (~35 km) over the Pocklington Rise. The crust thins to ~25 km in a basin to the south of the rise. A second ridge is located at 10.65°S, with a crustal thickness of ~35 km. A series of smaller rifted blocks are present approaching the continent-ocean boundary, with crustal thicknesses range from ~10 to ~25 km. Spreading segment 2 of the oceanic crust outcrops between 10.3°S and 10.25°S. The thickness of the oceanic crust is ~10 km. To the north of the continent-ocean boundary, continental crust thickens to ~12 km due to an isolated continental fault block. Oceanic crust (spreading segment 1) outcrops between 10.15°S and 10.02°S. The thickness of the oceanic crust is ~9 km. To the north of the continent-ocean boundary, continental crust is ~15 km thick. Oceanic crust again outcrops between 9.85°S and 9.8°S, and it is about ~11 km thick. To the north of the continent-ocean boundary, crustal thickness increases from ~13 to ~30 km a series of normal faults up-stepping to the north. Further north, the crust thins to ~25 km due to a large basin. To the north of this, the crust thickens to ~35 km over the Woodlark Rise and Woodlark Island. It decreases gradually to ~31 km toward the north of the rise due to the gradual slope.

Line 200:

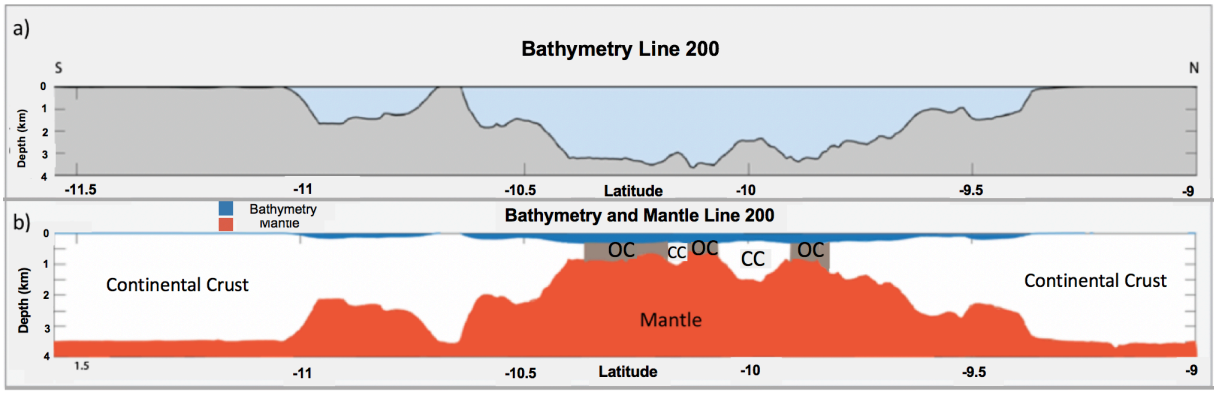

Figure B6. As Figure B1 but for seismic reflection line 200.

The southernmost portion of line 200 (Figure B6) has thick crust (~35 km) over the Pocklington Rise. The crust thins to ~20 km in a basin to the south of the rise. A second ridge is located at 10.7°S, with a crustal thickness of ~35 km. A series of smaller rifted blocks are present approaching the continent-ocean boundary, with crustal thicknesses ranging from ~10 to ~25 km. Spreading segment 2 of the oceanic crust outcrops between 10.3°S to 10.2°S. The thickness of the oceanic crust is ~10 km. To the north of the continent-ocean boundary, continental crust thickens to ~12 km due to an isolated continental fault block. Oceanic crust (spreading segment 1) outcrops between 10.1°S and 10.05°S. The thickness of the oceanic crust is ~9 km. To the north of the continent-ocean boundary, continental crust is ~15 km thick. Oceanic crust again outcrops between 9.9°S and 9.85°S, and it is about ~10 km thick. To the north of the continent-ocean boundary, crustal thickness increases from ~10 to ~30 km over a series of grabens. Further north, the crust thins to ~25 km due to a large basin. Past the basin, the crust thickens to ~35 km over the Woodlark Rise and Woodlark Island.